28th Bled Workshop @ 2025

NNU · 南京师范大学
NANJING NORMAL UNIVERSITY

Detecting Light Dark Matter with Plasmons

Lei Wu

in collaboration with Z.L. Liang, L.L. Su, B. Zhu

PRL 134 (2025) 7, 071001
2501.07591

Outline

- From WIMPs to Light Dark Matter (LDM)
- Electronic Collective Excitations: Plasmons
- Detecting LDM with Plasmons
- Conclusions

1. From WIMPs to Light DM

天文学观测

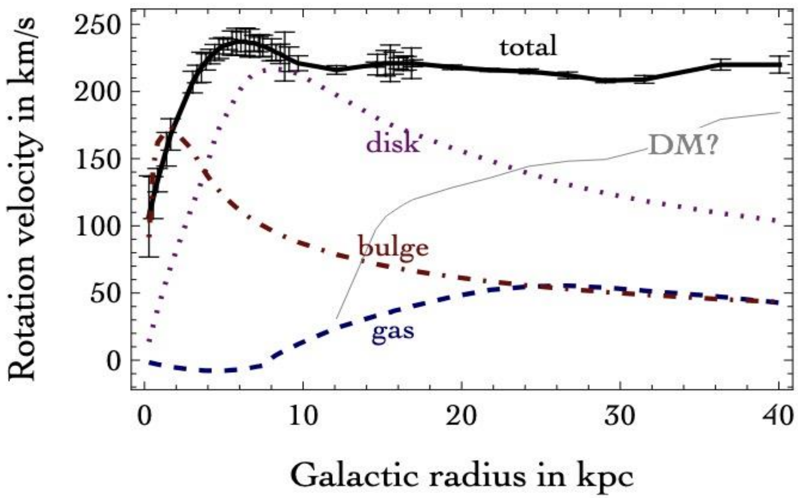

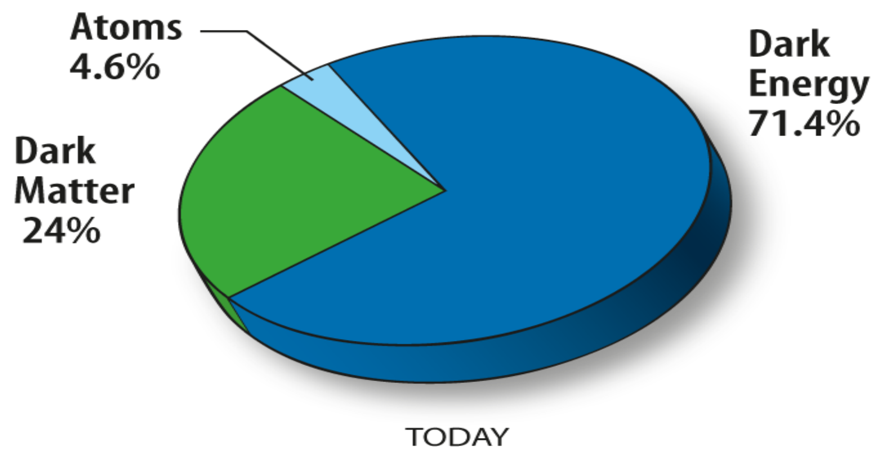

宇宙学观测

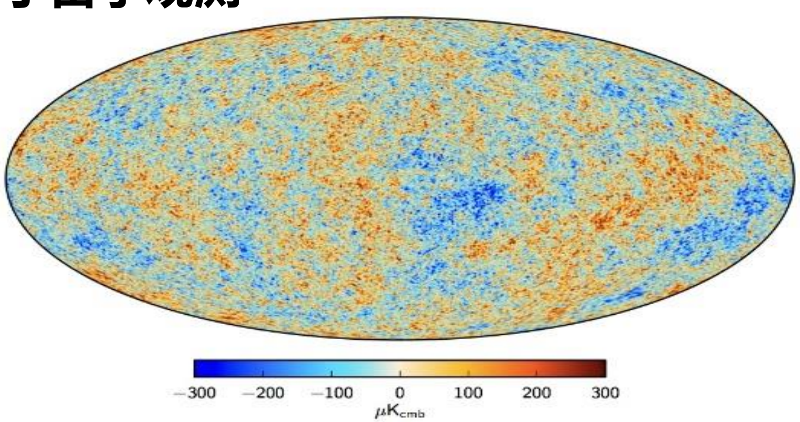

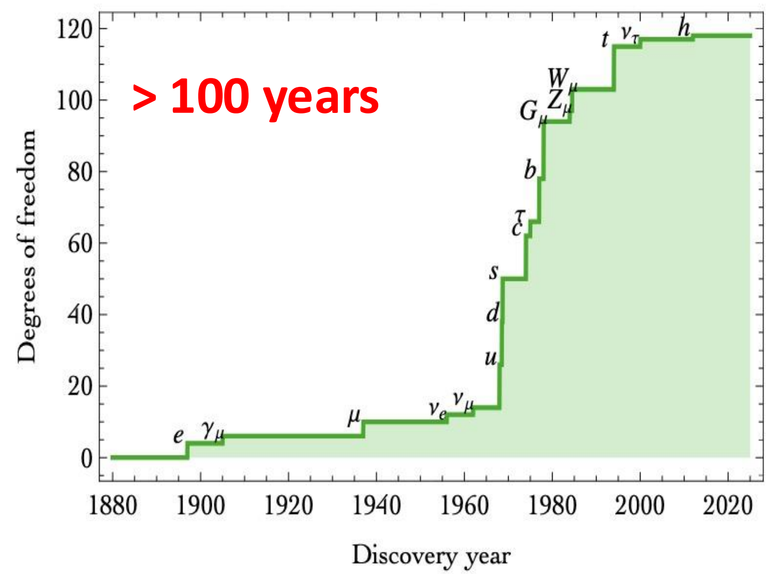

Dark Matter

???
years

……

1. From WIMPs to Light DM

天体物理	Primordial BH	1966, 1971	Zeldovich & Novikov, Hawking
	MACHOs	1981, 1986	Petrou; Paczynski
粒子物理	Gravitinos	1981, 1982	Fayet; Witten; Pagel & Primack
	Axions	1983	Preskill, Wise & Wilczek
	Neutralinos	1984	Ellis et al.
	Strangelets	1984	Witten; Fahri & Jaffe
	Q-balls	1984	Witten
	Extra-dimensional DM	1984	Kolb & Slansky; Servant & Tait
	WIMPs	1985	Steigman & Turner
	Sterile neutrinos	1993	Dodelson & Widrow
	Fuzzy DM	2000	Hu, Barkana & Gruzinov
	Sub-GeV DM	2003	Boehm, Fayet et al.

Relic Abundance

Solution to Big problems

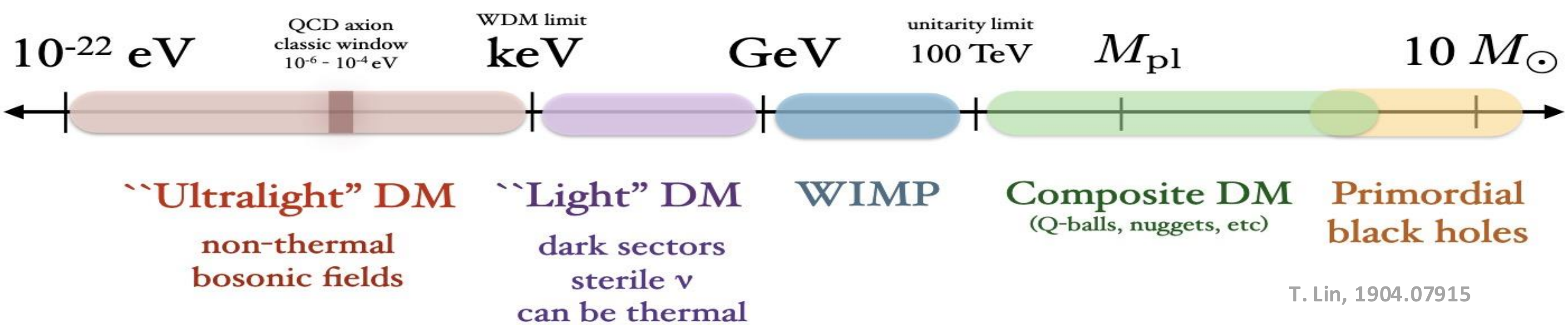

T. Lin, 1904.07915

1. From WIMPs to Light DM

WIMPs

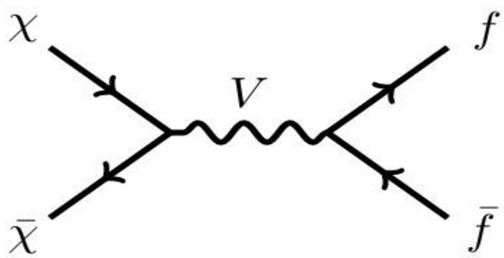

$m_\chi \sim 100$ GeV, $g_\chi \sim 0.6 \rightarrow \Omega_\chi \sim 0.1$

PandaX collaboration, 2402.03596

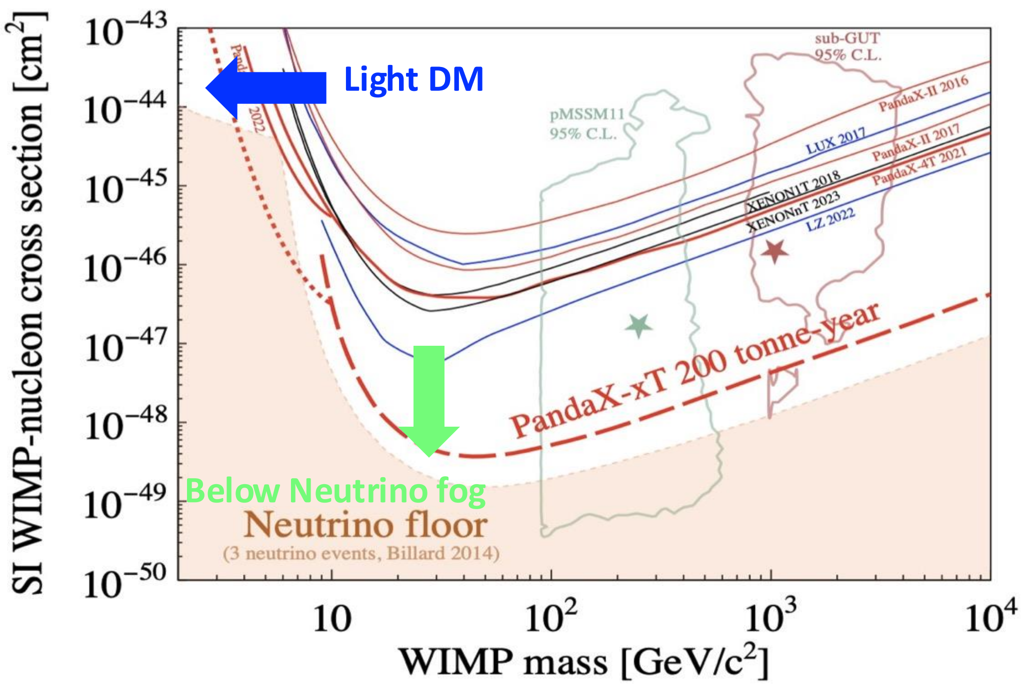

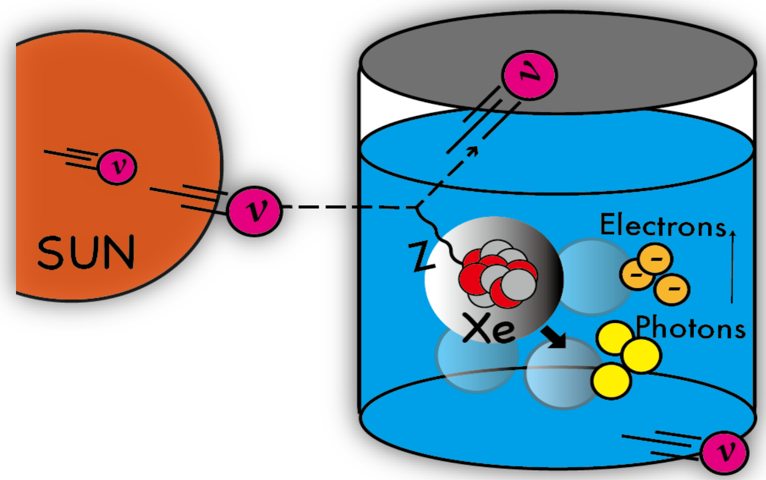

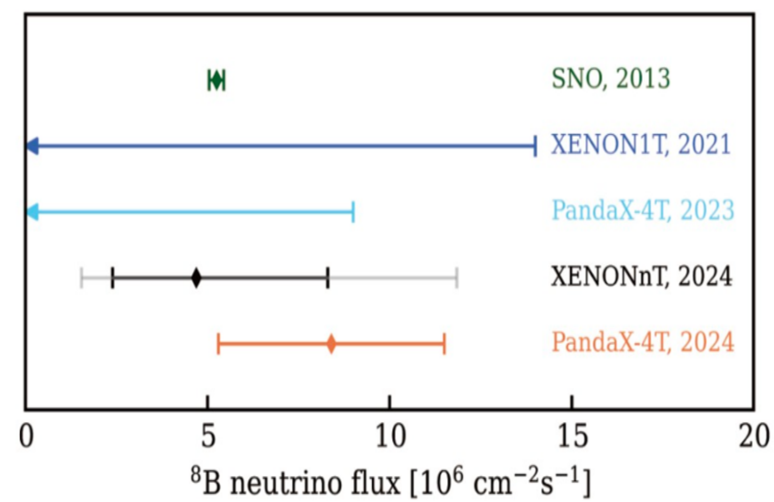

1. From WIMPs to Light DM

Light DM

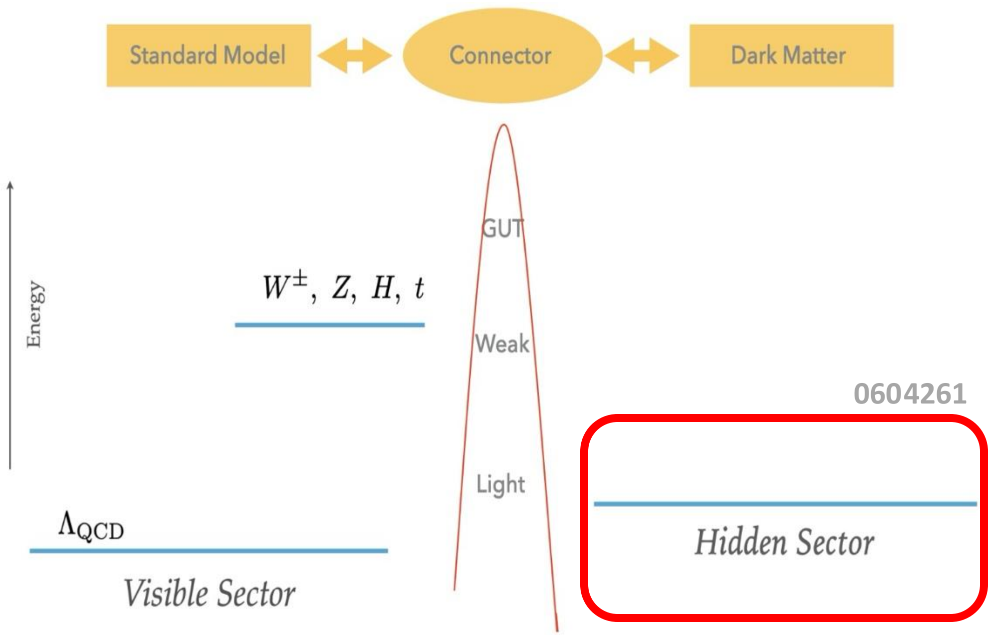

+

- SIMPs [YH, Kuflik, Volansky, Wacker, 2014; YH, Kuflik, Murayama, Volansky, Wacker, 2015]
- ELDERs [Kuflik, Perelstein, Rey-Le Lorier, Tsai, 2016 & 2017]

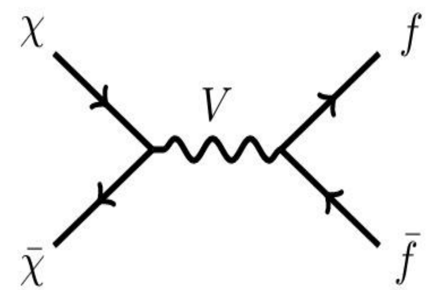

- $m_V > m_\chi \qquad \langle \sigma v \rangle \simeq \dfrac{16\pi \alpha_\chi \alpha_f m_\chi^2}{m_V^4}$

0305261
0711.4866
0803.4196

Light non-SM mediator

- $m_V < m_\chi \qquad \langle \sigma v \rangle \simeq \dfrac{\pi \alpha_\chi \alpha_f}{m_\chi^2}$

Data

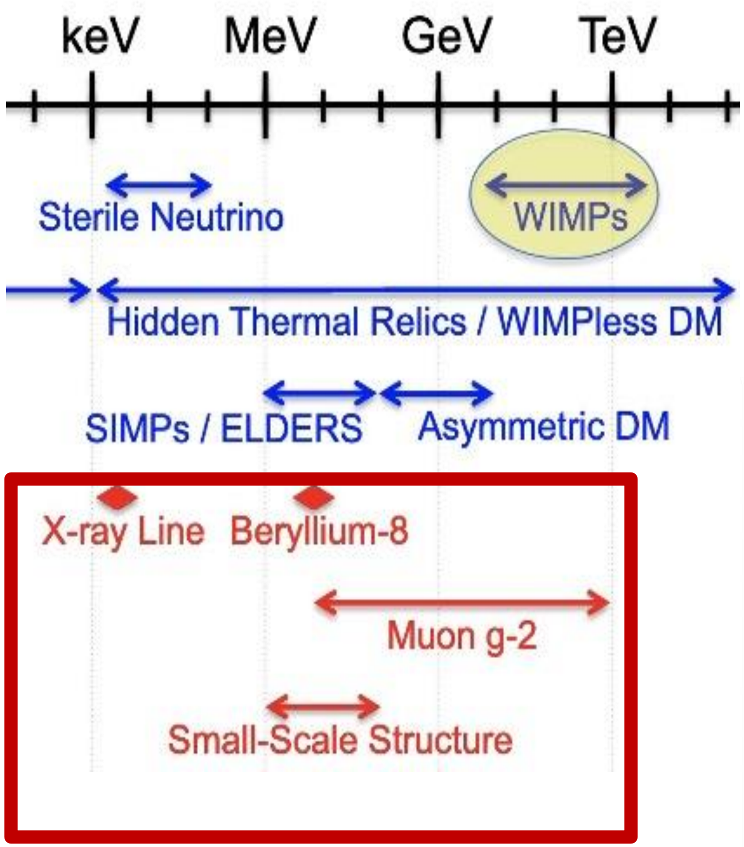

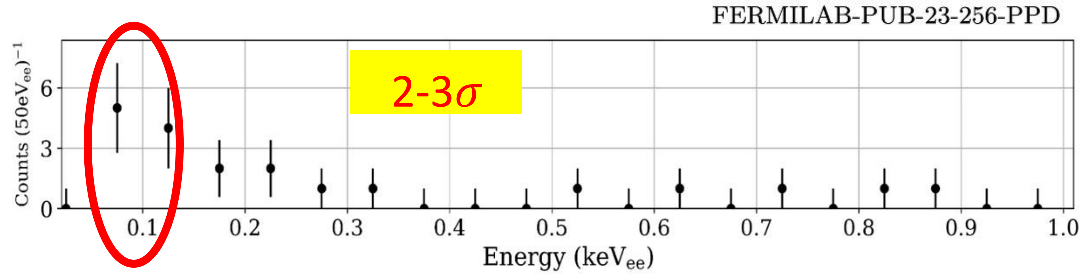

2002.06937

Readout Type	Target	Resolution	Exposure	Threshold	Excess Rate (Hz/kg)	Depth	Reference
Charge (E_e)	Ge	1.6 e^-	80 g·d	0.5 eVee ($\sim 1e^-$)[a]	[20, 100]	.7 km	EDELWEISS [6]
	Si	$\sim$0.2 e^-	0.18 g·d	1.2 eVee ($<1\,e^-$)	[6, 400]	100 m	SENSEI [4]
	Si	0.1 e^-	0.5 g·d	1.2 eVee ($<1\,e^-$)	[10, 2000]	~1 m	CDMS HVeV [3]
	Si	1.6 e^-	200 g·d	1.2 eVee ($\sim 1e^-$)	[1×10^{-3}, 7]	2 km	DAMIC [7]
Energy (E_{det})	Ge	18 eV	200 g·d	60 eV	>2	~1 m	EDELWEISS [1]
	$CaWO_4$	4.6 eV	3600 g·d	30 eV	$>3\times10^{-3}$	.4 km	CRESST-III [2]
	Al_2O_3	3.8 eV	0.046 g·d	20 eV	>30	~1 m	νCLEUS [8]
Photo e^-	Xe	6.7 PE ($\sim 0.25\,e^-$)	15 kg·d	12.1 eVee (~14 PE)	[0.5, 3] $\times10^{-4}$	.4 km	XENON10 [5, 9]
	Xe	6.2 PE ($\sim 0.31\,e^-$)	30 kg·yr	~70 eVee (~80 PE)	$>2.2\times10^{-5}$	.4 km	XENON100 [5]
	Xe	<10 PE	60 kg·yr	~140 eVee (~90 PE)	$>1.7\times10^{-6}$	.4 km	XENON1T [10]
	Ar	~15 PE ($\sim 0.5\,e^-$)	6780 kg·d	50 eVee	$>6\times10^{-4}$	.4 km	Darkside50 [11]

1. From WIMPs to Light DM

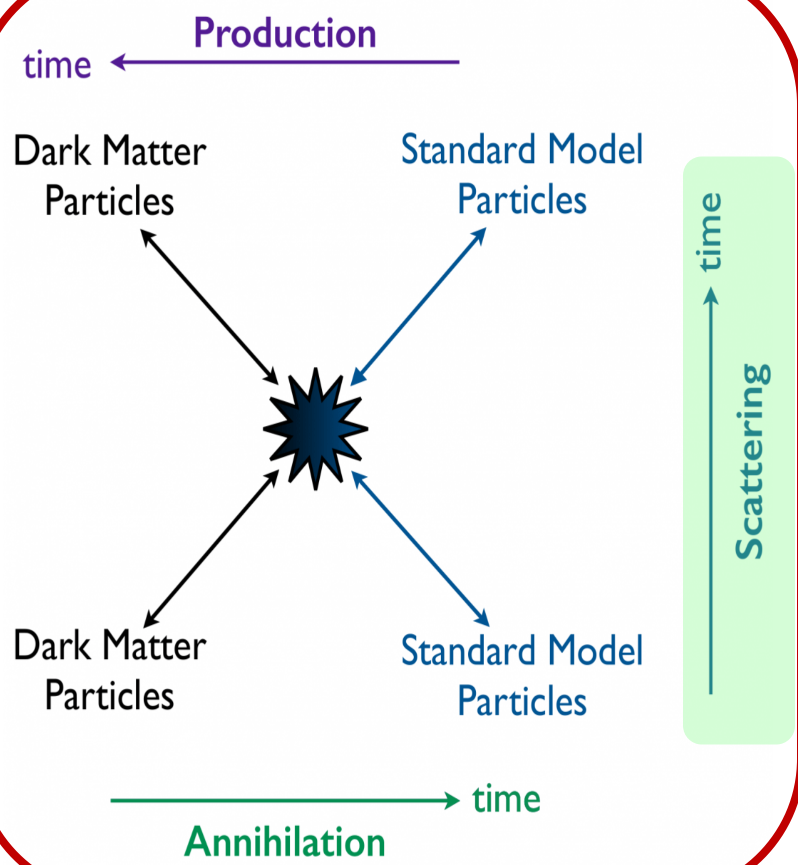

- BBN, CMB
- Large Scale Structure
- Stellar Evolution and Cooling
- Meson decays
- Colliders

2. Electronic Collective Excitations : Plasmons

PHYSICAL REVIEW D VOLUME 9, NUMBER 5 1 MARCH 1974

Coherent effects of a weak neutral current

Daniel Z. Freedman†
National Accelerator Laboratory, Batavia, Illinois 60510
and Institute for Theoretical Physics, State University of New York, Stony Brook, New York 11790
(Received 15 October 1973; revised manuscript received 19 November 1973)

If there is a weak neutral current, then the elastic scattering process $\nu + A \to \nu + A$ should have a sharp coherent forward peak just as $e + A \to e + A$ does. Experiments to observe this peak can give important information on the isospin structure of the neutral current. The experiments are very difficult, although the estimated cross sections (about 10^{-38} cm^2 on carbon) are favorable. The coherent cross sections (in contrast to incoherent) are almost energy-independent. Therefore, energies as low as 100 MeV may be suitable. Quasi-coherent nuclear excitation processes $\nu + A \to \nu + A^*$ provide possible tests of the conservation of the weak neutral current. Because of strong coherent effects at very low energies, the nuclear elastic scattering process may be important in inhibiting cooling by neutrino emission in stellar collapse and neutron stars.

PHYSICAL REVIEW D VOLUME 31, NUMBER 12

Detectability of certain dark-matter candidates

Mark W. Goodman and Edward Witten
Joseph Henry Laboratories, Princeton University, Princeton, New Jersey 08544
(Received 7 January 1985)

We consider the possibility that the neutral-current neutrino detector recently proposed by Drukier and Stodolsky could be used to detect some possible candidates for the dark matter in galactic halos. This may be feasible if the galactic halos are made of particles with coherent weak interactions and masses $1-10^6$ GeV; particles with spin-dependent interactions of typical weak strength and masses $1-10^2$ GeV; or strongly interacting particles of masses $1-10^{13}$ GeV.

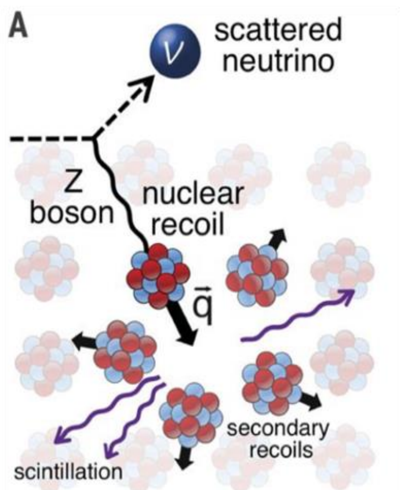

D. Akimov et al, Science 357 (2017)

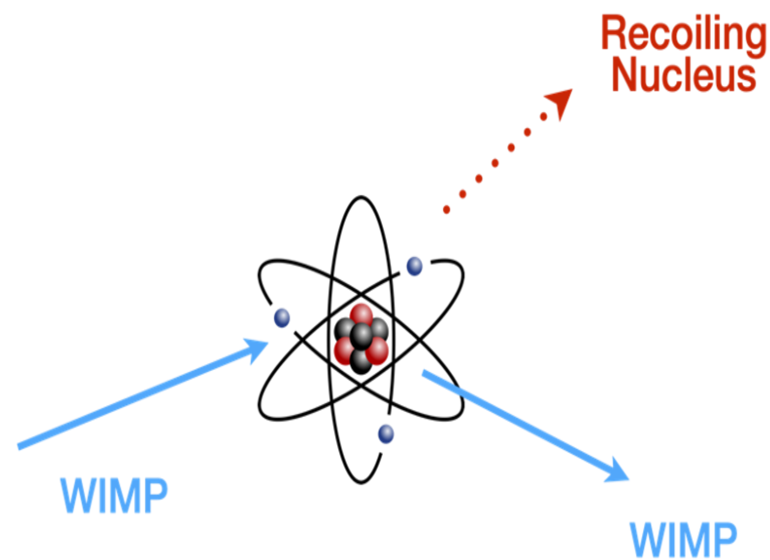

2. Electronic Collective Excitations : Plasmons

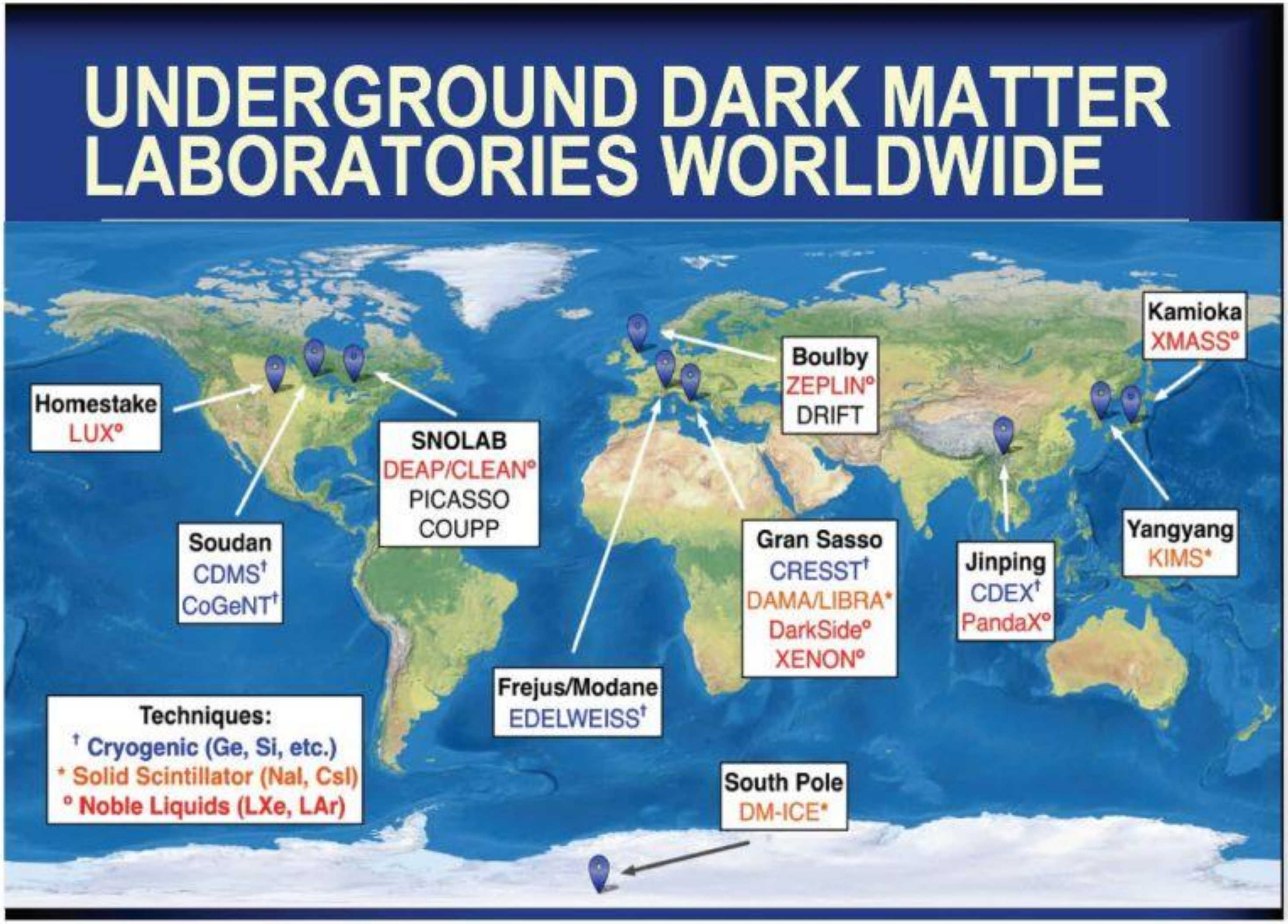

2. Electronic Collective Excitations : Plasmons

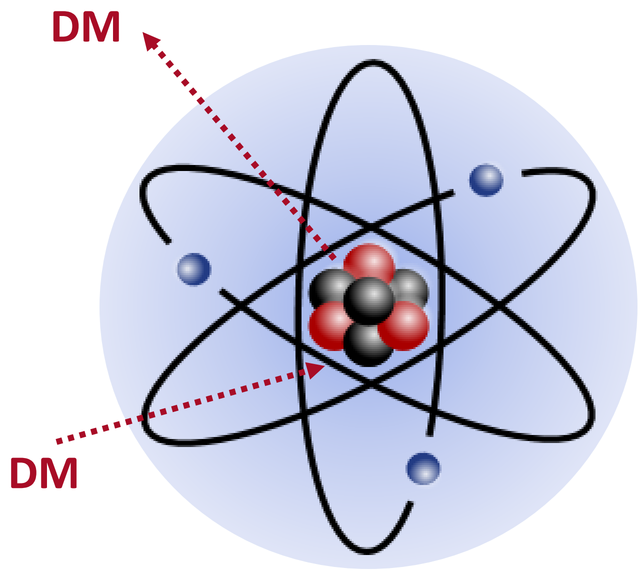

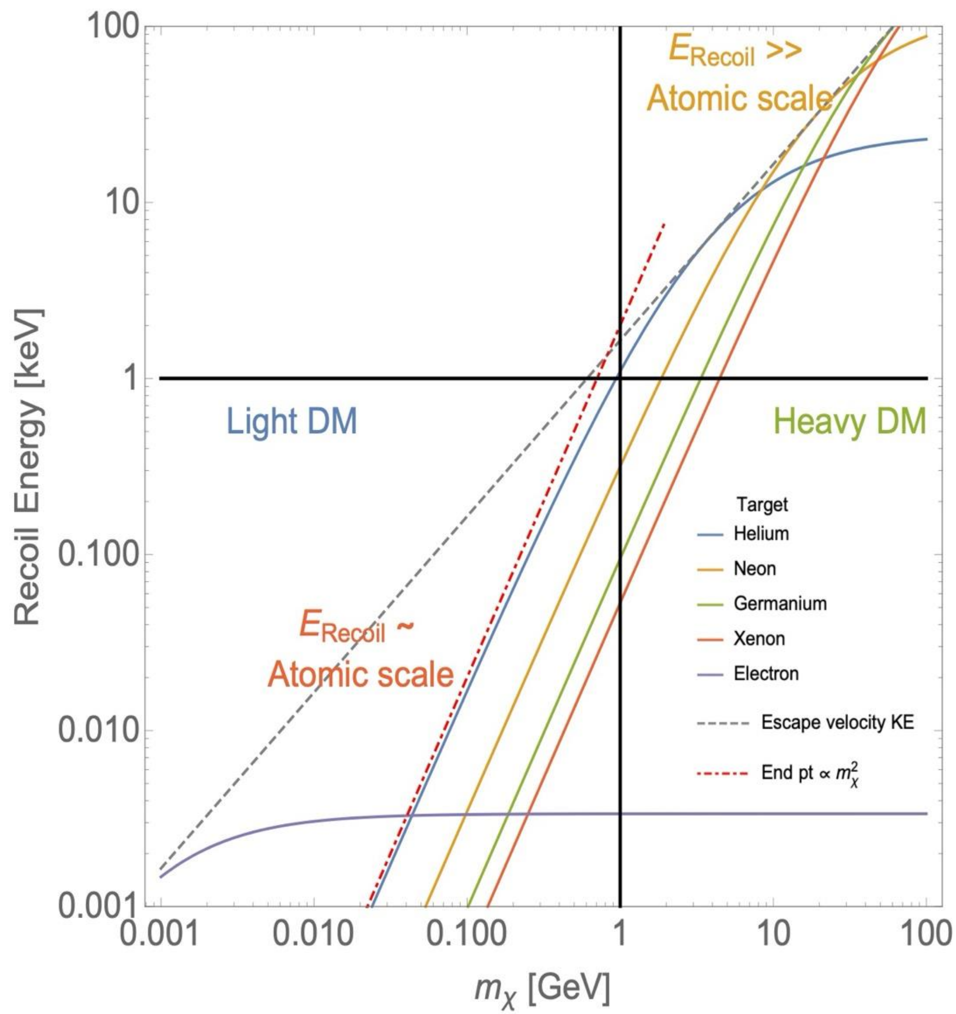

$$E_R = \frac{q^2}{2m_A} = \frac{1}{2} m_\chi v^2 \left(\frac{4 m_\chi m_A}{(m_A^2 + m_\chi^2)} \right) \cos^2 \theta_R$$

2. Electronic Collective Excitations : Plasmons

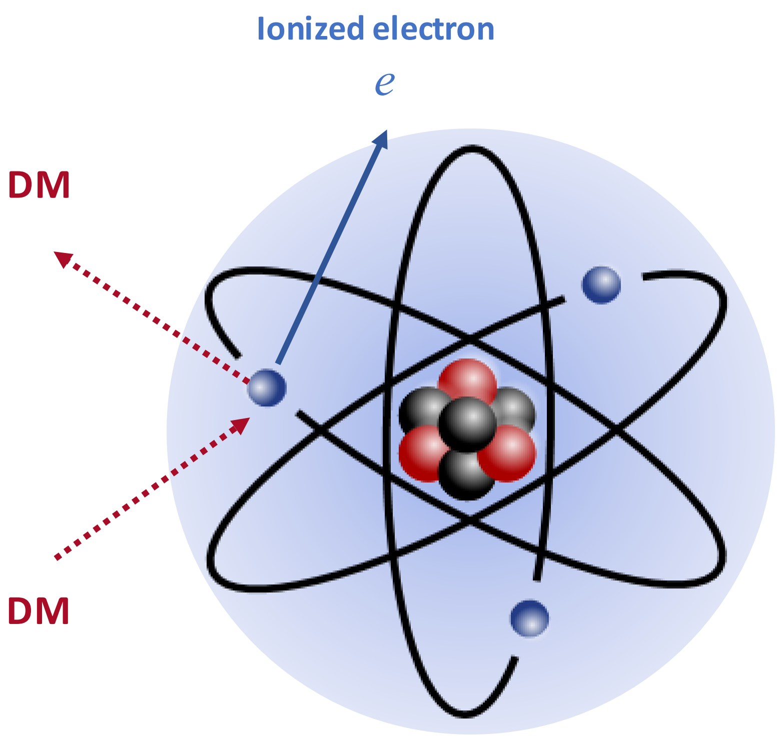

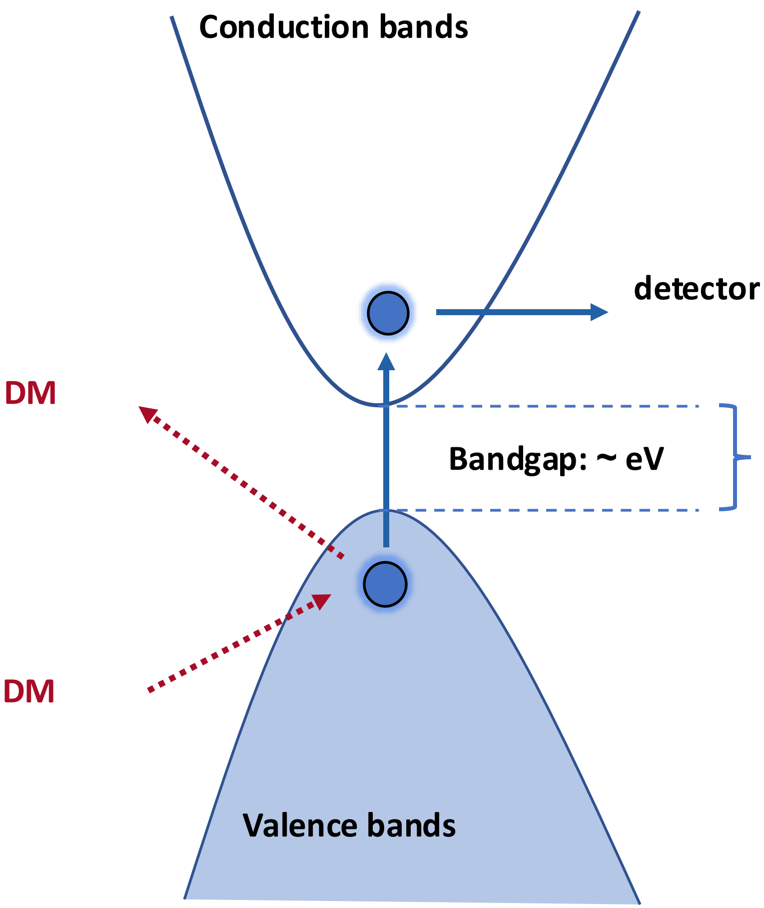

2. Electronic Collective Excitations: Plasmons

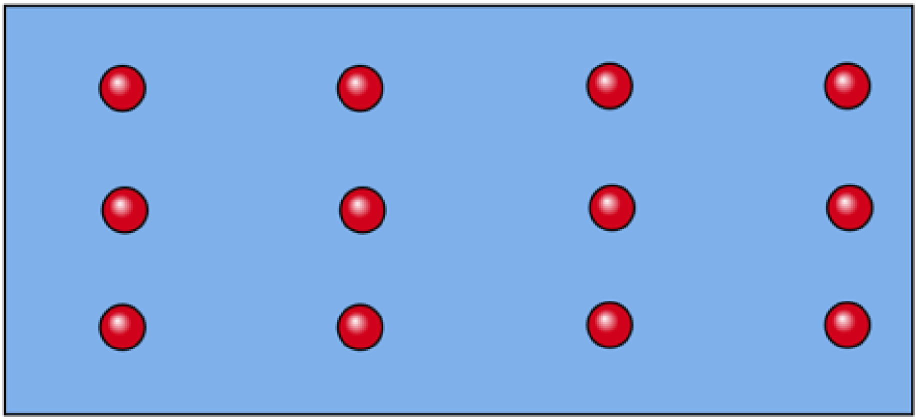

electron gas

+

ionic lattice

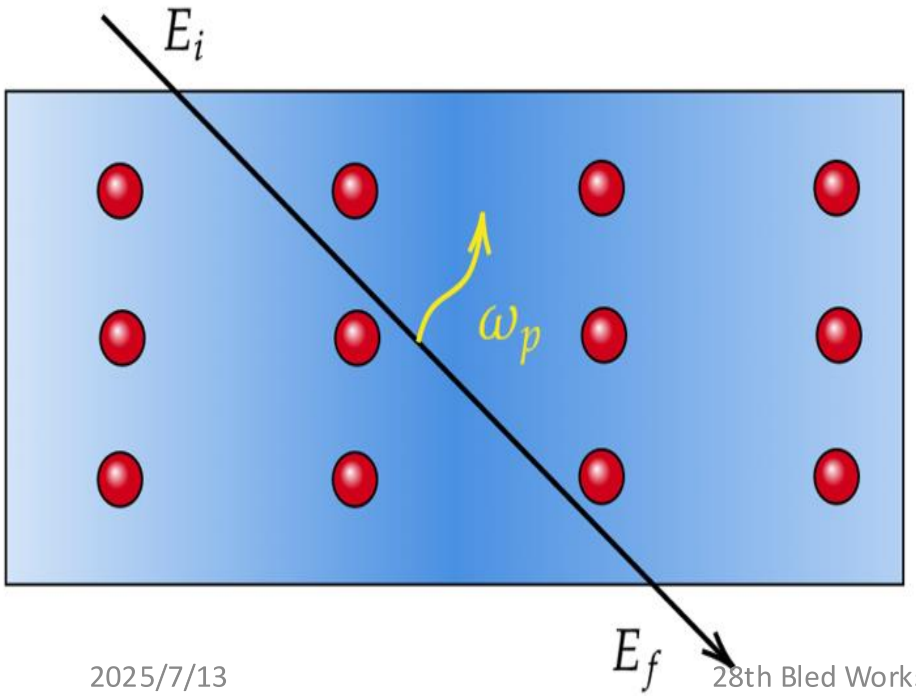

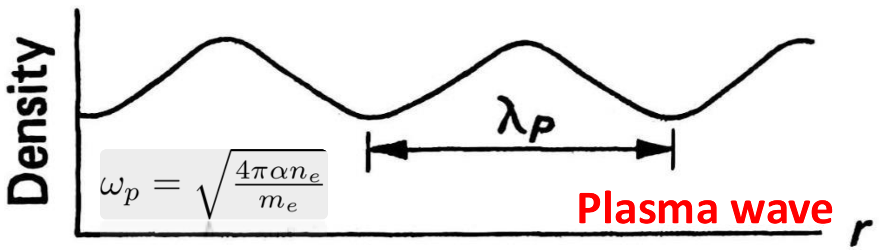

Plasmon

quanta of electron density fluctuation

2. Electronic Collective Excitations: Plasmons

How to identify plasmons: Electron Energy Loss Spectroscopy (EELS)

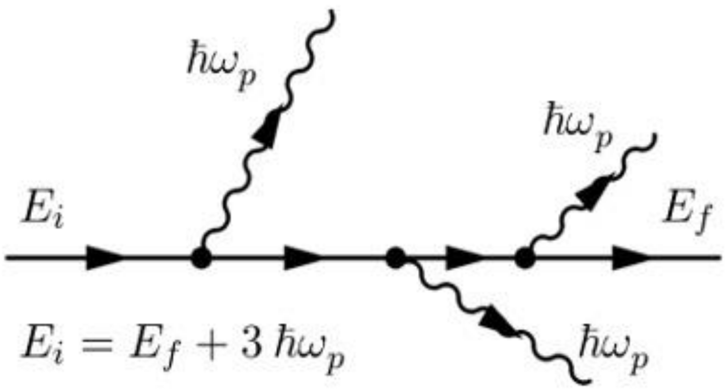

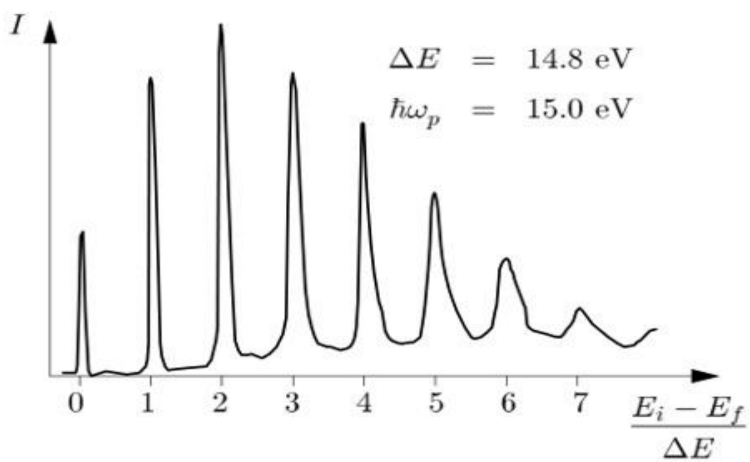

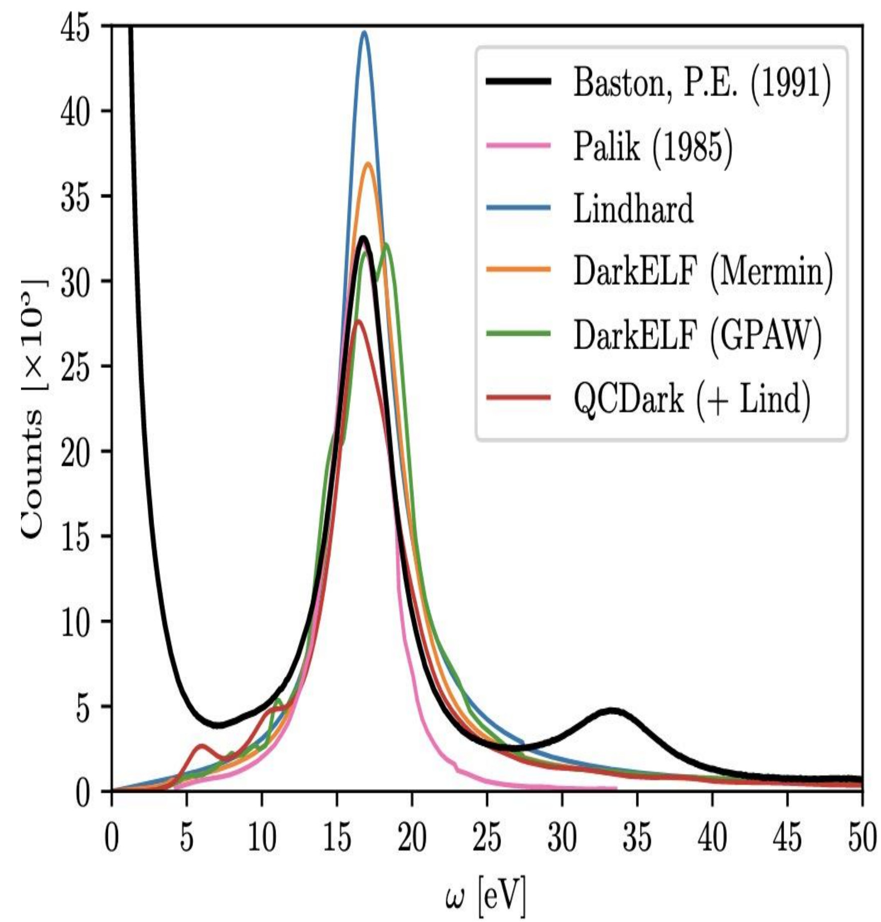

3. Detecting LDM with Plasmons

DM-induced Plasmon Signals in Solid Detector

$$R \sim \int d^3\mathbf{v} f(\mathbf{v}) \int d^3\mathbf{q} F^2_{\mathrm{DM}}(\mathbf{q}) S\left(\mathbf{q}, \omega_{\mathbf{q}}\right)$$

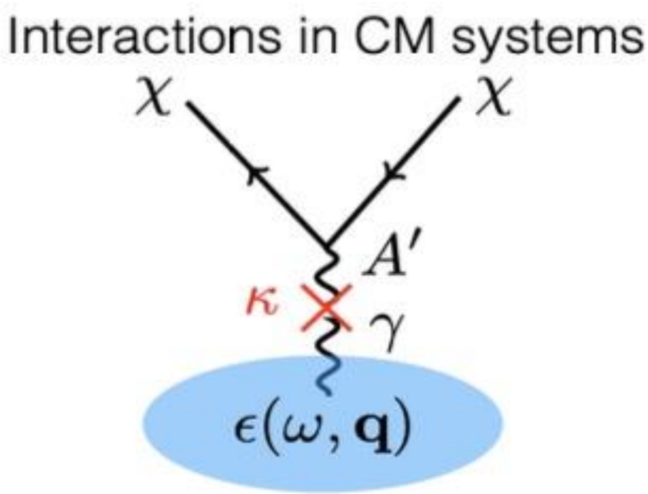

Dielectric Function

Electronic Structure (polarization)

↑

$$\varepsilon(Q,\omega) = \varepsilon_1(Q,\omega) + i\varepsilon_2(Q,\omega)$$

↓

Dissipation Processes (absorption and scattering)

3. Detecting LDM with Plasmons

Simplified Model :

$$\mathcal{L}_{\rm int} \supset g_\chi \bar{\chi}\gamma^\mu \chi A'_\mu + g_e \bar{e}\gamma^\mu e A'_\mu$$

Feynman Rules (Solid Physics):

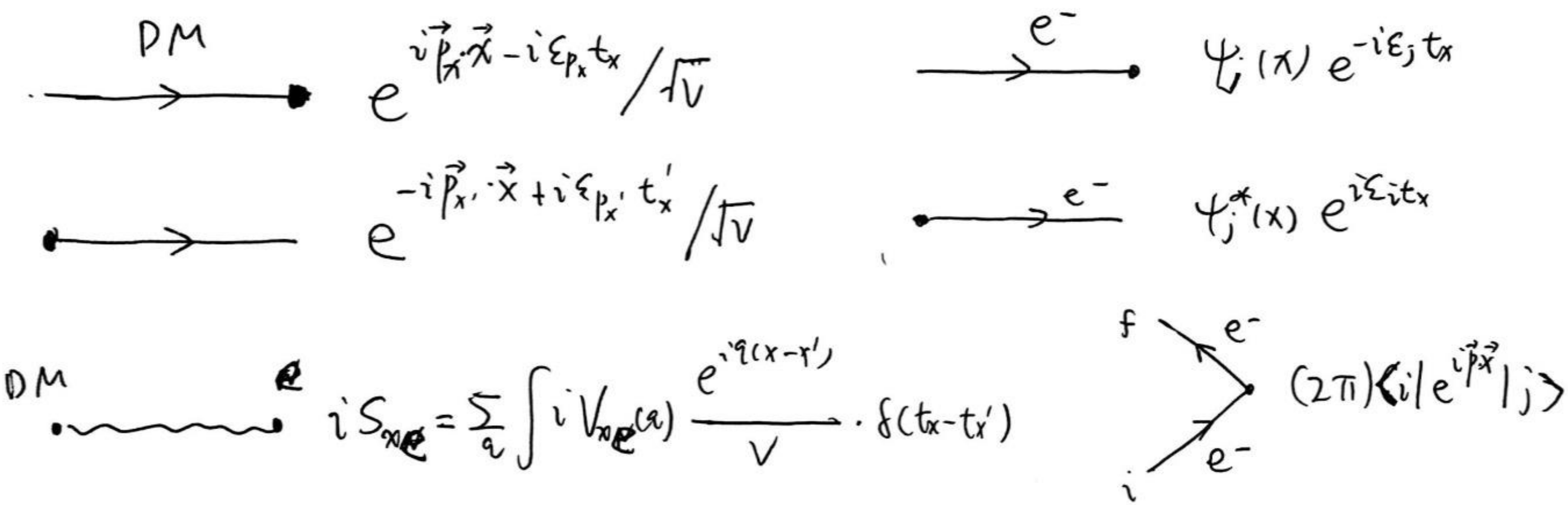

3. Detecting LDM with Plasmons

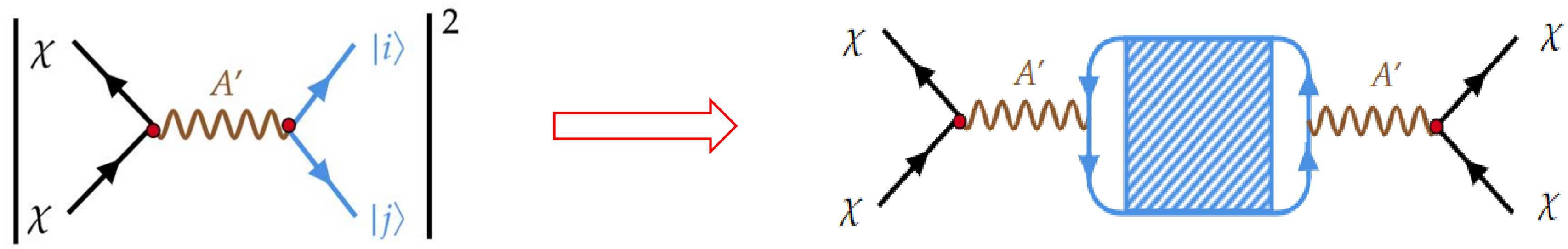

Energy Loss Function (ELF)

$$\Gamma(\mathbf{p}_\chi) = \int \frac{d^3\mathbf{Q}}{(2\pi)^3} |V(\mathbf{Q},\omega)|^2 \left[2\frac{Q^2}{e^2}\mathrm{Im}\left(-\frac{1}{\epsilon(\mathbf{Q},\omega)}\right)\right],$$

DM scattering rate

Scattering potential

$$\mathrm{Im}\left[\frac{-1}{\epsilon}\right] = \frac{\mathrm{Im}[\epsilon]}{\mathrm{Re}[\epsilon]^2 + \mathrm{Im}[\epsilon]^2}$$

$$\frac{1}{\pi}\frac{\frac{1}{2}\Gamma}{(x-x_0)^2 + \left(\frac{1}{2}\Gamma\right)^2} \sim \delta(x - x_0)$$

3. Detecting LDM with Plasmons

Liang, Su, LW, Zhu, PRL 134 (2025) 7, 071001

Dielectric Function

$$\frac{1}{\epsilon(\mathbf{Q},\omega)} = 1 + V_e(Q)\,\chi^{\mathrm{r}}_{\hat{\rho}\hat{\rho}}(\mathbf{Q},\omega)$$

$\chi^{\mathrm{r}}_{\hat{\rho}\hat{\rho}} =$

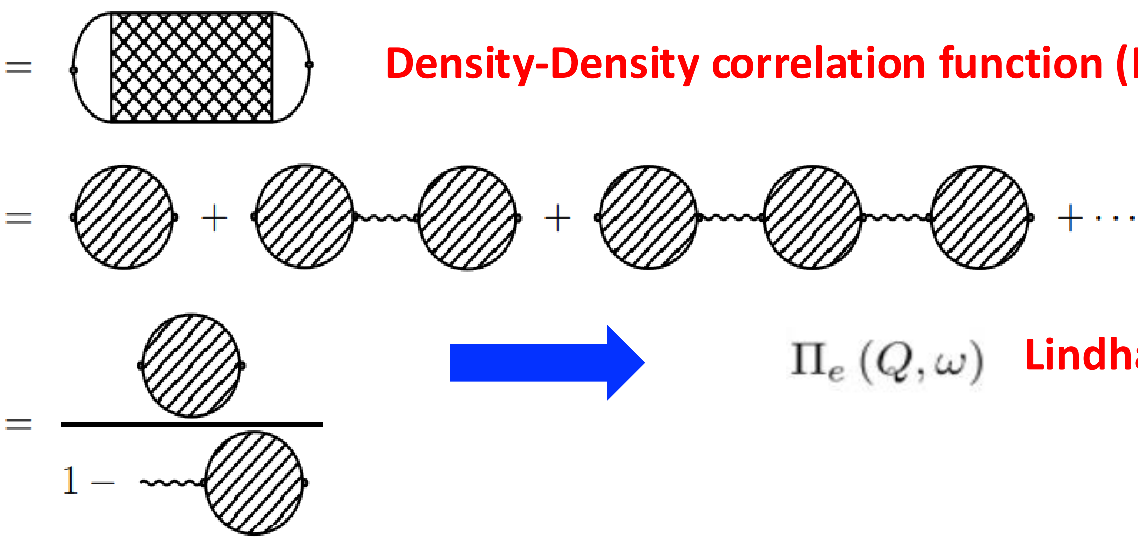

Density-Density correlation function (RPA)

$$= \frac{\Pi_e}{1 - V_e\,\Pi_e},$$

$\Pi_e(Q,\omega)$ **Lindhard function**

3. Detecting LDM with Plasmons

Liang, Su, LW, Zhu, PRL 134 (2025) 7, 071001

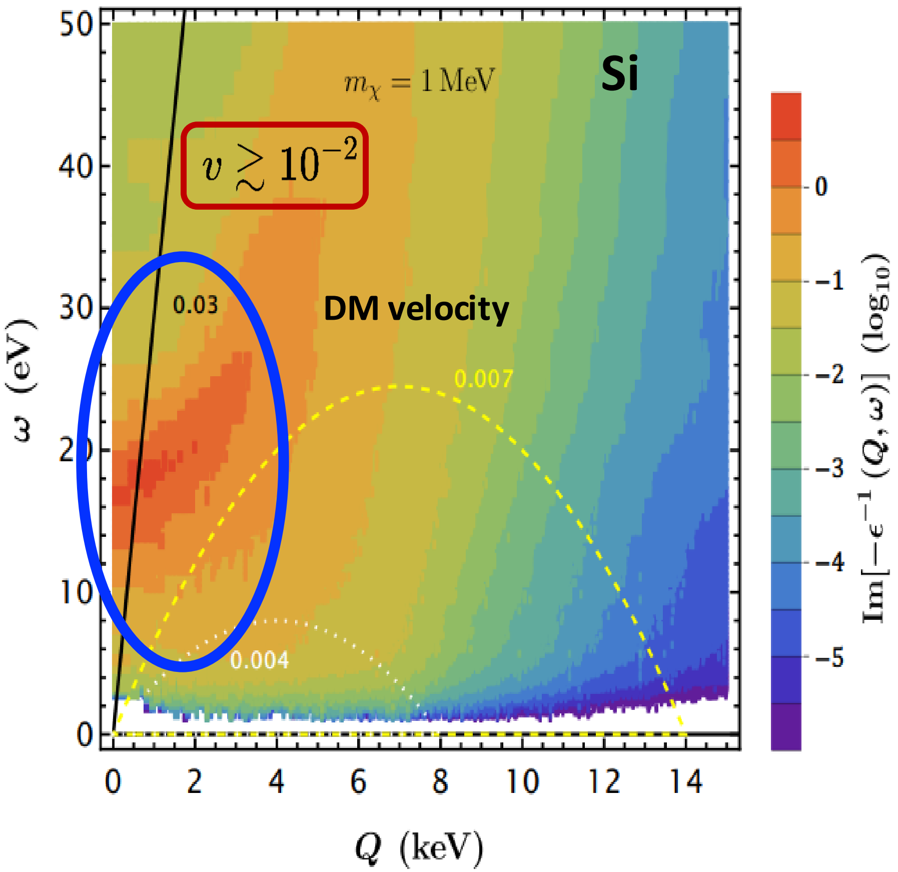

- **Energy Loss Function:**

  Density Functional Theory

- **Resonance (plasmon) :**

  $|Q| < 5$ keV, $\omega \sim 15$ eV

- **To excite plasmon:**

  $V_{min} > q/\omega$

Low deposited energy

Fast-moving DM

2. Electronic Collective Excitations : Plasmons

SENSEI, DAMIC, CONNIE

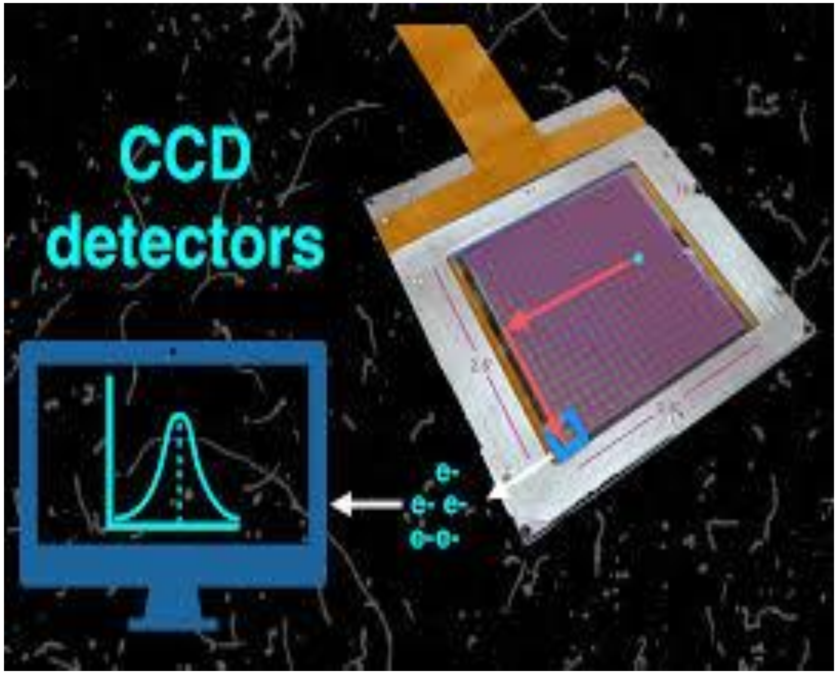

Electron recoil ionizing 1–6 e^- in the detector, which corresponds to (~1.2–20 eV) energy depositions

3. Detecting LDM with Plasmons

Cosmic Ray

1810.07705
1810.10543

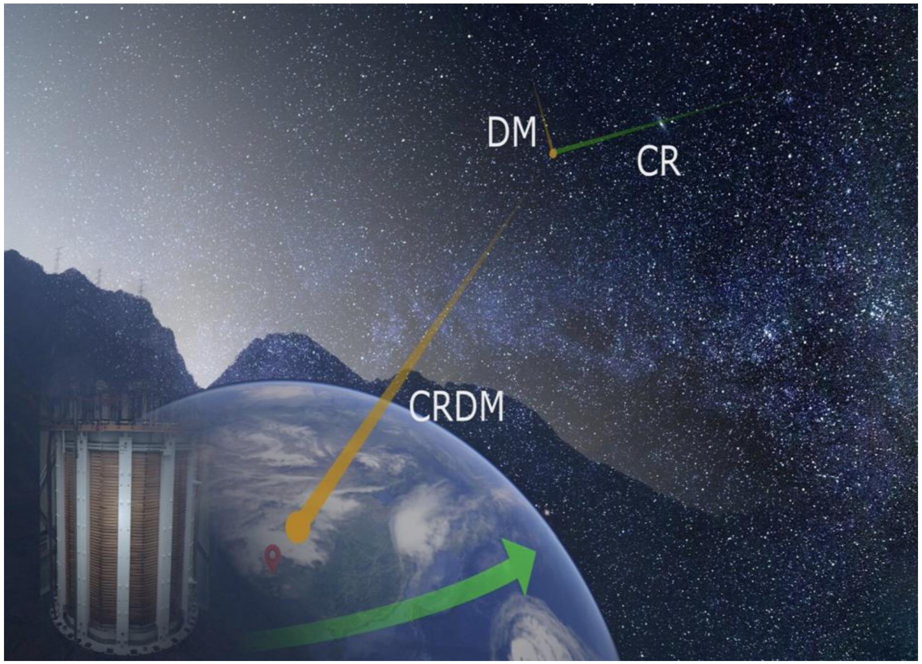

Supernova Neutrino

0908.1790
1506.03825
2501.07591

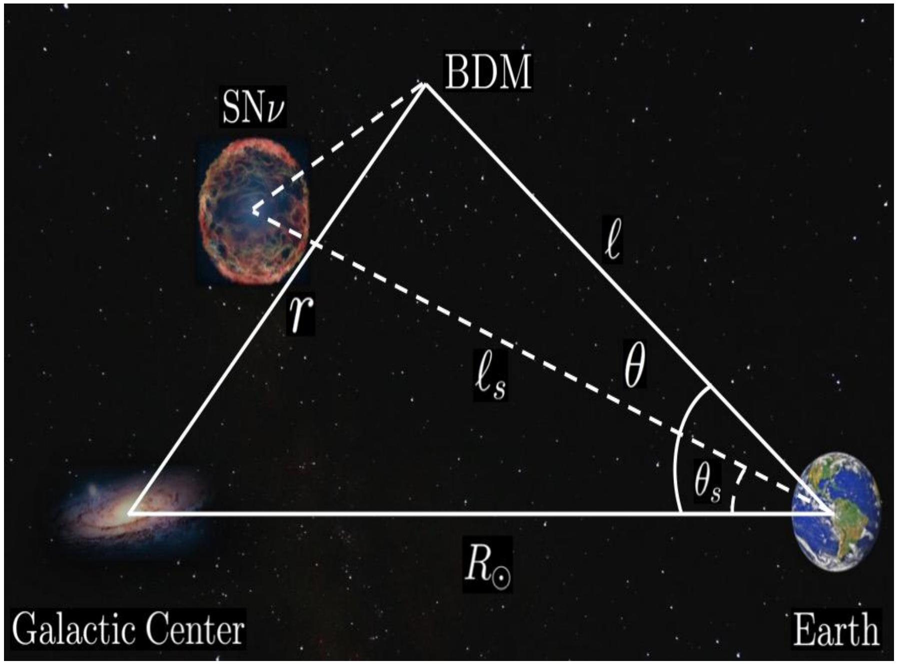

3. Detecting LDM with Plasmons

Liang, Su, LW, Zhu, PRL 134 (2025) 7, 071001

Cosmic Ray Boosted DM

$$\frac{d\Phi_\chi}{dT_\chi} = \int \frac{d\Omega}{4\pi} \int_{\rm l.o.s.} \frac{\rho_\chi(\Omega,\ell)}{m_\chi} d\ell \int_{T_e^{\rm min}}^{+\infty} dT_e \frac{d\sigma_{\chi e}}{dT_\chi} \frac{d\Phi_e}{dT_e}$$

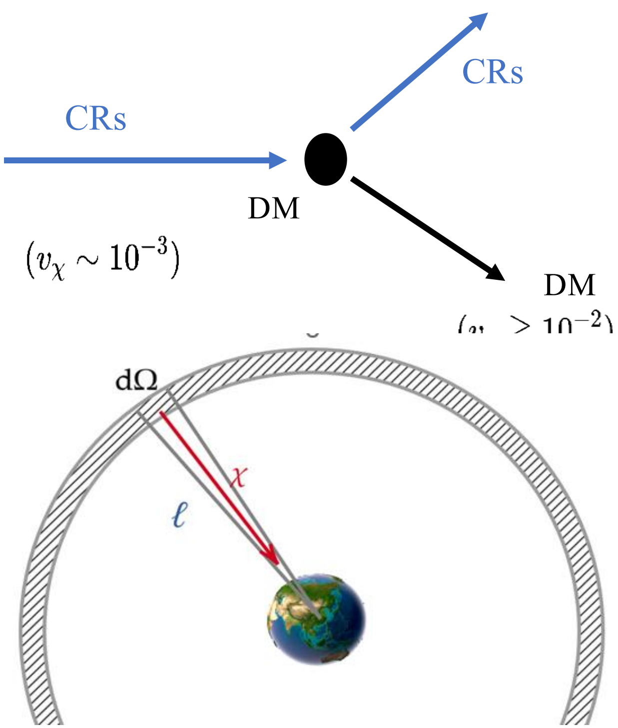

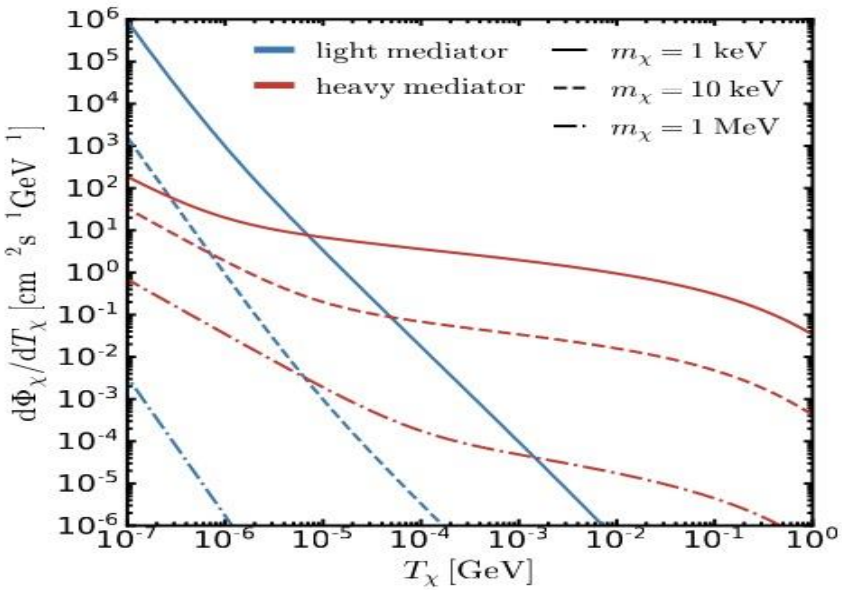

$$R = \frac{1}{\rho_T} \int dT_\chi \int \frac{d\Omega}{4\pi} \frac{d\Phi_\chi}{dT_\chi} \left(\frac{E_\chi}{p_\chi}\right) \Gamma(p_\chi)$$

3. Detecting LDM with Plasmons

Liang, Su, LW, Zhu, PRL 134 (2025) 7, 071001

$$|F_{\rm DM}(q)|^2 = \frac{(\alpha^2 m_e^2 + m_{A'}^2)^2}{(q^2 + m_{A'}^2)^2} = \begin{cases} 1 & \text{heavy mediator} \\ \frac{(\alpha m_e)^4}{q^4} & \text{light mediator} \end{cases}$$

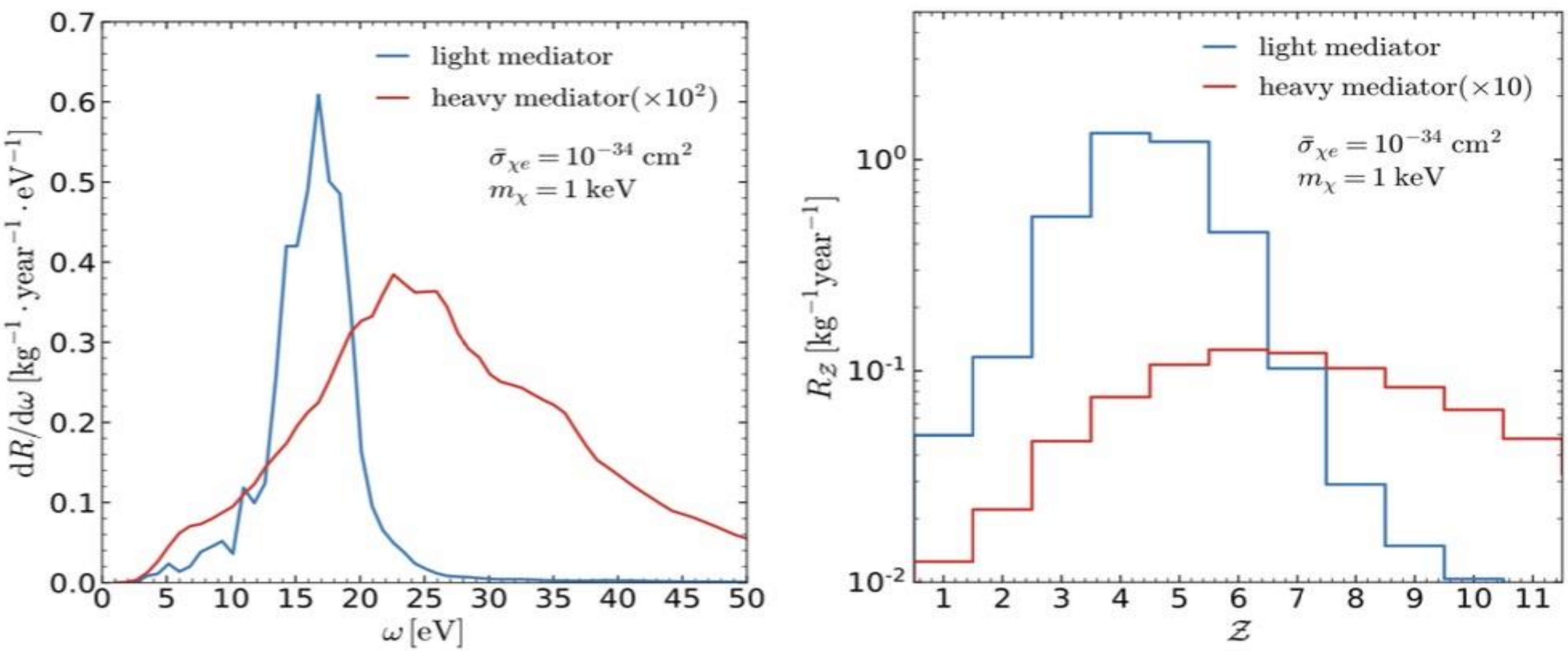

3. Detecting LDM with Plasmons

2312.13342

SENSEI @ SNOLAB (100.72 g.days)

	All data		
Shape	Expo.	Ev.	Bkgd.
2e2p, h	13.58	10	10.66
2e2p, v	16.21	13	12.65
2e2p, d	17.82	32	25.31
2e, all	**46.61**	**55**	**48.62**
3e2p	30.87	3	0.01
3e3p	26.84	1	0.06
3e, all	**57.71**	**4**	**0.07**
4e2p	19.51	0	0.00
4e3p	27.60	0	0.00
4e4p	15.93	0	0.00
4e, all	**63.03**	**0**	**0.00**
5e, all	65.56	0	0.00
6e, all	67.31	0	0.00
7e, all	68.53	0	0.00
8e, all	69.52	0	0.00
9e, all	70.30	0	0.00
10e, all	70.89	0	0.00

Liang, Su, LW, Zhu, PRL 134 (2025) 7, 071001

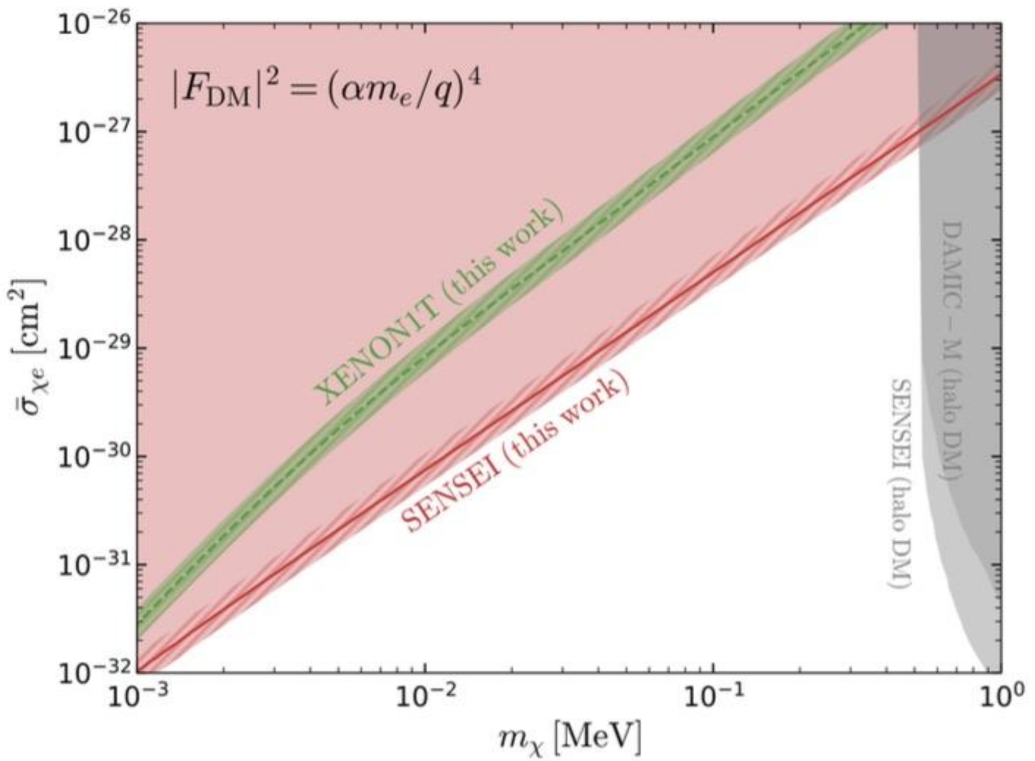

Light Dark Matter	Noble Liquid Detector (large volume, high threshold)	Solid detector (small volume, low threshold)
Non-Relativistic	✔	✔
Relativistic	✔	**Collective Excitations**

Conclusions

Dark Matter Particle

Direct Detection

(~ 40 years, 9 orders)

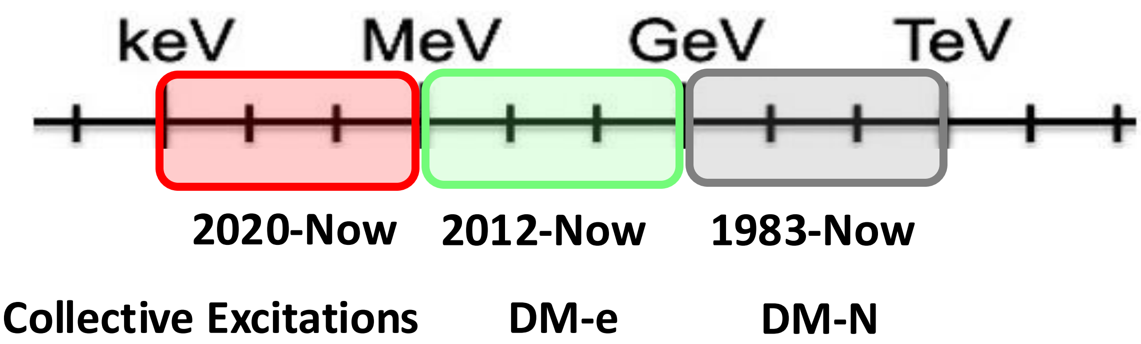

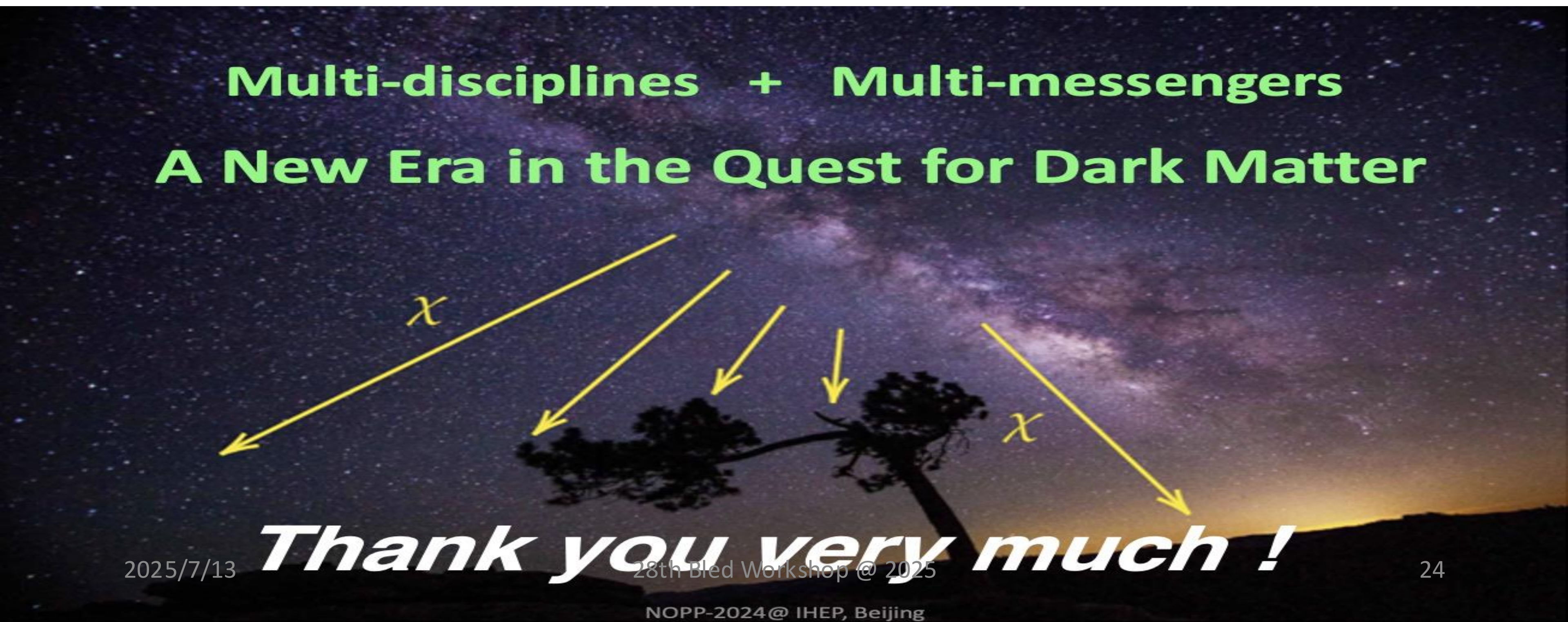

DD experiments of DM

Name	Detector	Target	Active Mass	Fiducial Live Exposure	Status	Start Ops (after construction)	End Ops	Location of Experiment
XMASS	Scintillator	LXe	832 kg		Ended	2010	2019	Kamioke
XENON100	TPC	LXe	62 kg		Ended	2012	2016	LNGS
XENON1T	TPC	LXe	1,995 kg		Ended	2017	2019	LNGS
XENON1T (Ionization)	TPC Ioniz.-only	LXe	1,995 kg		Ended	2017	2019	LNGS
XENONnT	TPC	LXe	7,000 kg	20 t yr	Construction	2021	2025	LNGS
LUX	TPC	LXe	250 kg	30,000 kg d	Ended	2013	2016	SURF
LUX (Ionization)	TPC Ioniz.-only	LXe	250 kg		Ended	2017	2019	SURF
LZ	TPC	LXe	8,000 kg	20 t yr	Construction	2021	2025	SURF
PandaX-II	TPC	LXe	580 kg		Ended	2016	2018	CJPL
PandaX-4T	TPC	LXe	4,000 kg	20 t yr	Construction	2021	2025	CJPL
LZ HydroX	TPC	LXe+H2	8,000 kg		R&D	2026		SURF
Darwin / US G3	TPC	LXe	40,000 kg	200 t yr	Planning	2028	2033	LNGS / SURI
DEAP-3600	Scintillator	LAr	3,300 kg		Running	2016	202X	SNOLAB
DarkSide-50	TPC	LAr	46 kg	46 kg year	Ended	2013	2019	LNGS
Darkside-LM (Ionization)	TPC Ioniz.-only	LAr	46 kg		Ended	2018	2019	LNGS
Darkside-20k	TPC	LAr	30 t	200 t yr	Construction	2025	2030	LNGS
ARGO	TPC	LAr	300 t	3000 t yr	Planning	2030	2035	SNOLAB
DAMA/LIBRA	Scintillator	NaI	250 kg		Running	2003		LNGS
ANAIS-112	Scintillator	NaI	112 kg	Goal 5 years	Running	2017	2022	Canfranc
COSINE-100	Scintillator	NaI	106 kg		Running	2016	2021	YangYang
COSINE-200	Scintillator	NaI	200 kg		Construction	2022	2025	YangYang
COSINE-200 South Pole	Scintillator	NaI	200 kg		Planning	2023	?	South Pole
COSINUS	Bolometer Scintillator	NaI	?		Planning	2023	?	LNGS
SABRE PoP	Scintillator	NaI	5 kg		Construction	2021	2022	LNGS
SABRE (North)	Scintillator	NaI	50 kg		Planning	2022	2027	LNGS
SABRE (South)	Scintillator	NaI	50 kg		Planning	2022	2027	SUPL
CDEX-10	Ionization (77K)	Ge	10 kg	103 kg d	Running	2016	?	CJPL
CDEX-100 / 1T	Ionization (77K)	Ge	100-1000 kg		Planning	202X		CJPL
SuperCDMS	Cryo Ionization	Ge	9 kg		Ended	2011	2015	Soudan
CDMSLite (High Field)	Cryo Ionization	Ge	1.4 kg	~75 kg d	Ended	2012	2015	Soudan
CDMS-HVeV Si	Cryo Ionization HV	Si	0.9 g	0.5 g d	Ended	2018	2018	SNOLAB
SuperCDMS CUTE	Cryo Ionization / HV	Ge/Si	5 kg/1 kg		Construction	2020	2022	SNOLAB
SuperCDMS SNOLAB	Cryo Ionization / HV	Ge/Si	11 kg/3 kg		Construction	2023	2028	SNOLAB
EDELWEISS III	Cryo Ionization	Ge	20 kg		Ended	2015	2018	LSM
EDELWEISS III (High Field)	Cryo Ionization HV	Ge	33 g		Running	2019		LSM
CRESST-II	Bolometer Scintillation	CaWO4	5 kg		Ended	2012	2015	LNGS
CRESST-III	Bolometer Scintillation	CaWO4	240 g		Ended	2016	2018	LNGS
CRESST-III (HW Tests)	Bolometer Scintillation	CaWO4			Running	2020		LNGS
PICO-2	Bubble Chamber	C3F8	2 kg		Ended	2013	2015	SNOLAB
PICO-40	Bubble Chamber	C3F8	35 kg		Construction	2020		SNOLAB
PICO-60	Bubble Chamber	CF3I,C3F8	52 kg		Ended	2013	2017	SNOLAB
PICO-500	Bubble Chamber	C3F8	430 kg		Construction	2021		SNOLAB
DRIFT-II	Gas Directional	CF4	0.14 kg		Ended			Boulby
NEWAGE-03b'	Gas Directional	CF4	14 g	4.5 kg d	Ended	2013	2017	
NEWS-G	Gas Drift	CH4			Ended	2017	2019	LSM
NEWS-G	Gas Drift	CH4			Construction	2020	2025	SNOLAB
DAMIC	CCD	Si	2.9 g	0.6 kg d	Ended	2015	2015	SNOLAB
DAMIC	CCD	Si	40 g Si		Ended	2017	2019	SNOLAB
DAMIC100	CCD	Si	100 g Si		Not Built			SNOLAB
DAMIC-M	CCD Skipper	Si	1 kg Si		Construction	2021	2024	LSM
SENSEI	CCD Skipper	Si	2 g Si	2g x 24 d	Running	2019	2020	Fermilab u/g
SENSEI	CCD Skipper	Si	100 g Si		Construction	2021	2023	SNOLAB

Lower Mass of DM at detectors

$$\frac{1}{2} m_\chi v_\chi^2 \gtrsim E_{\text{threshold}} \quad \Rightarrow \quad m_\chi \gtrsim 6\ \text{MeV} \cdot \left(\frac{E_{\text{threshold}}}{15\ \text{eV}}\right)$$

Threshold	Lowest DM Mass Probed	Relevant Techniques, Technologies, and Materials
20 eV	20 MeV (ER) 100 MeV (NR)	Noble Elements (TPCs & SPCs) Solid-State Charge Detectors Phonon Detectors Threshold Detectors
500 meV	1 MeV (ER/NR) 500 meV (Abs.)	Semiconductor Detectors Athermal Phonon Detectors Scintillators NIR Photon Detectors
5 meV	10 keV (CE) 5 meV (Abs.)	Superconductors Low-Gap Materials Athermal Phonon Detectors Polar Materials Superfluids FIR Photon Detectors Magnetic Bubble Chambers Other new ideas

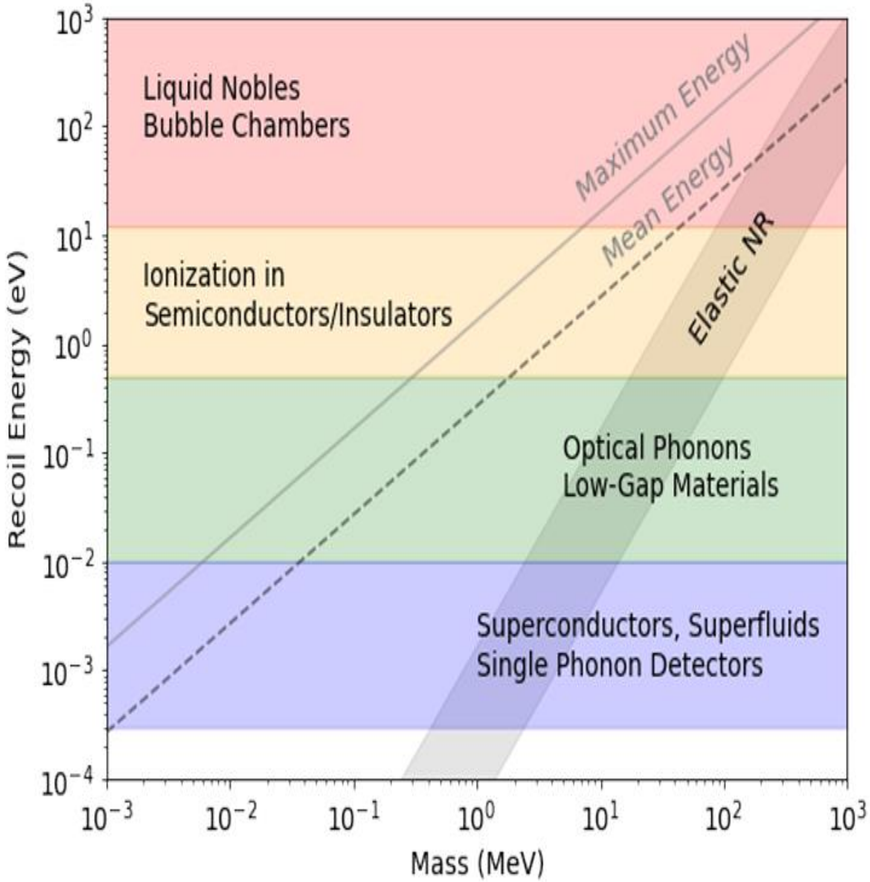

Rouven Essig, *et.al*, arxiv: 2203.08297

Electron Density Fluctuation

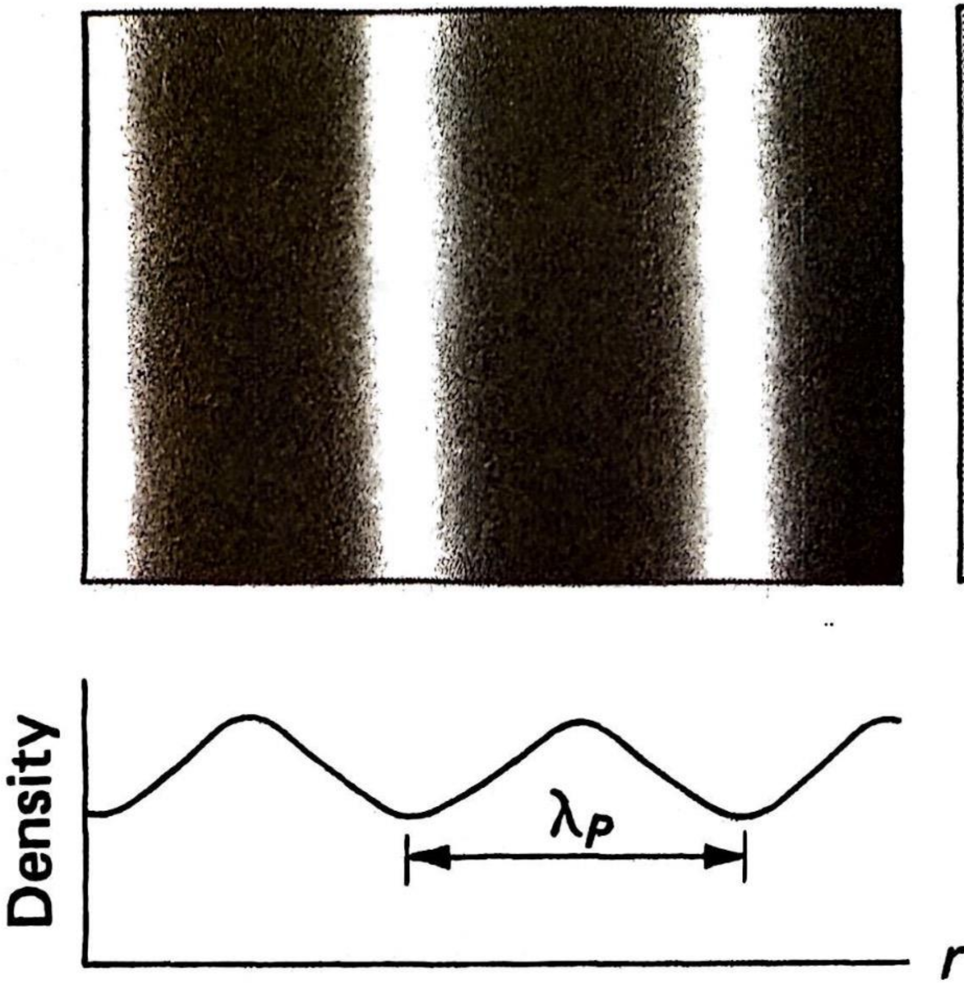

Plasma Wave in Electron Gas

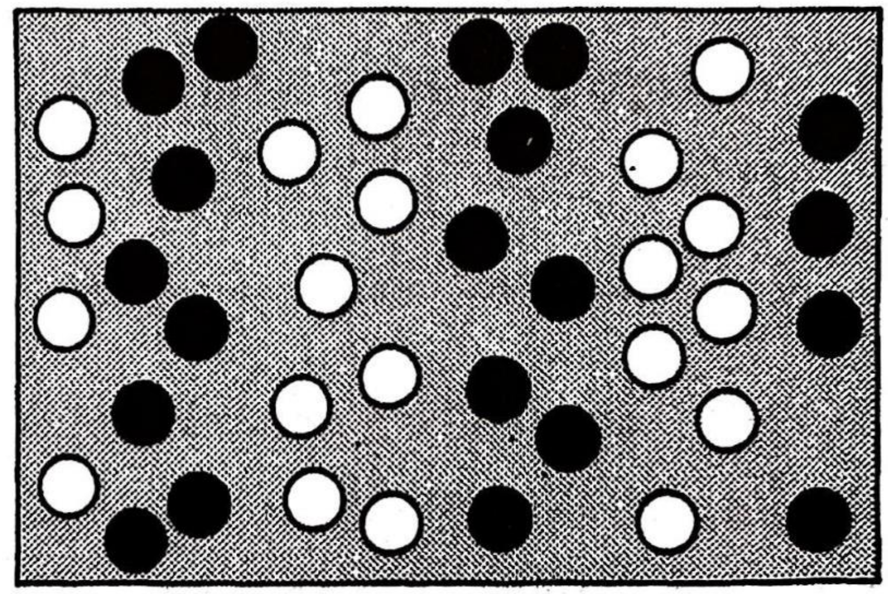

Electron- Particle hole Picture of Plasma Wave

$$\hat{\psi}(\mathbf{x}) = \sum_k \hat{a}_k u_k(\mathbf{x})$$

$$\int \mathrm{d}^3 x e^{i\mathbf{Q}\cdot\mathbf{x}} u_i^*(\mathbf{x})\, u_j(\mathbf{x})$$

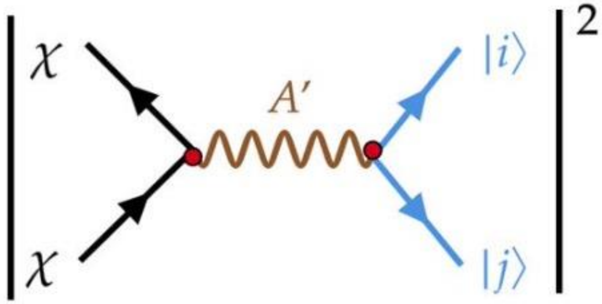

$$\sum_{i,j} p_j \langle j|e^{-i\mathbf{Q}\cdot\hat{\mathbf{x}}}|i\rangle \underline{\langle i|e^{i\mathbf{Q}\cdot\hat{\mathbf{x}}}|j\rangle}$$

$$\langle i|e^{i\mathbf{Q}\cdot\hat{\mathbf{x}}}|j\rangle = \int \mathrm{d}^3 x e^{i\mathbf{Q}\cdot\mathbf{x}} \left\langle i|\hat{\psi}^\dagger(\mathbf{x})\,\hat{\psi}(\mathbf{x})\,|j\right\rangle = \int \mathrm{d}^3 x e^{i\mathbf{Q}\cdot\mathbf{x}} \langle i|\hat{\rho}(\mathbf{x})\,|j\rangle$$

$$\int \mathrm{d}^3 x' \mathrm{d}^3 x e^{i\mathbf{Q}\cdot(\mathbf{x}-\mathbf{x}')} \sum_j p_j \langle j|\hat{\rho}(\mathbf{x}')\,\hat{\rho}(\mathbf{x})\,|j\rangle \quad \sim \left\langle \hat{\rho}\hat{\rho} \right\rangle$$

$$
\begin{aligned}
\sigma &= \sum_{i,f} \mathcal{P}_i \sigma_{i\to f} \\
&= \int \frac{\mathrm{d}^3 p'_\chi}{(2\pi)^3} \frac{1}{2} \sum_{s,s'} \bar{u}^{s'}_{p'_\chi} \gamma^0 u^s_{p_\chi} \bar{u}^s_{p_\chi} \gamma^0 u^{s'}_{p'_\chi} \frac{2\pi\delta(\omega_{pp'}-\omega)}{4E_\chi E'_\chi v_\chi} \sum_{i,f} \mathcal{P}_i \langle i | e^{-i\mathbf{Q}\cdot\hat{\mathbf{x}}} | f \rangle \langle f | e^{i\mathbf{Q}\cdot\hat{\mathbf{x}}} | i \rangle \\
&= \int \mathrm{d}\omega\, \delta(\omega + \varepsilon_i - \varepsilon_f) \int \mathrm{d}^3\mathbf{Q}\, \delta^{(3)}(\mathbf{Q} + \mathbf{p}'_\chi - \mathbf{p}_\chi) \int \frac{\mathrm{d}^3 p'_\chi}{(2\pi)^3} \frac{\pi\bar{\sigma}_{\chi e}[(E_\chi + E'_\chi)^2 - Q^2]}{4\mu^2_{\chi e} E_\chi E'_\chi v_\chi} \left(\frac{\alpha^2 m_e^2 + m^2_{A'}}{Q^2 - \omega^2 + m^2_{A'}} \right)^2 \\
&\times 2\pi\delta(\omega_{pp'}-\omega) \int \mathrm{d}^3\mathbf{x}\, \mathrm{d}^3\mathbf{x}' \sum_{i,f} \mathcal{P}_i \langle i | e^{-i\mathbf{Q}\cdot\hat{\mathbf{x}}'} \hat{\rho}_e | f \rangle \langle f | e^{i\mathbf{Q}\cdot\hat{\mathbf{x}}} \hat{\rho}_e | i \rangle \\
&= \int \mathrm{d}\omega \int \frac{\mathrm{d}^3\mathbf{Q}}{(2\pi)^3} \frac{\pi\bar{\sigma}_{\chi e}[(E_\chi + E'_\chi)^2 - Q^2]}{4\mu^2_{\chi e} E_\chi E'_\chi v_\chi} \left(\frac{\alpha^2 m_e^2 + m^2_{A'}}{Q^2 - \omega^2 + m^2_{A'}} \right)^2 2\pi\delta(\omega_{pp'}-\omega) \\
&\times \sum_{i,f} \mathcal{P}_i \langle i | \hat{\rho}_{\mathbf{Q}} | f \rangle \langle f | \hat{\rho}_{-\mathbf{Q}} | i \rangle\, \delta(\omega + \varepsilon_i - \varepsilon_f) \\
&= V_{\mathrm{target}} \int \mathrm{d}\omega \int \frac{\mathrm{d}^3\mathbf{Q}}{(2\pi)^3} \frac{\pi\bar{\sigma}_{\chi e}[(E_\chi + E'_\chi)^2 - Q^2]}{4\mu^2_{\chi e} E_\chi E'_\chi v_\chi} \left(\frac{\alpha^2 m_e^2 + m^2_{A'}}{Q^2 - \omega^2 + m^2_{A'}} \right)^2 \delta(\omega_{pp'}-\omega)\, S_{\hat{\rho}\hat{\rho}}(\mathbf{Q},\omega) \\
&= 2V_{\mathrm{target}} \int \mathrm{d}\omega \int \frac{\mathrm{d}^3\mathbf{Q}}{(2\pi)^3} \frac{\pi\bar{\sigma}_{\chi e}[(E_\chi + E'_\chi)^2 - Q^2]}{4\mu^2_{\chi e} E_\chi E'_\chi v_\chi} \left(\frac{\alpha^2 m_e^2 + m^2_{A'}}{Q^2 - \omega^2 + m^2_{A'}} \right)^2 \frac{\delta(\omega_{pp'}-\omega)}{V_{\mathrm{Cou}}(\mathbf{Q})} \mathrm{Im}\left[\frac{-1}{\epsilon(\mathbf{Q},\omega)} \right],
\end{aligned}
$$

where $V_{\mathrm{target}} = N_{\mathrm{cell}} V_{\mathrm{cell}}$ is the volume of the target material. In the third line, we insert two identities $\int \mathrm{d}\omega\, \delta(\omega + \varepsilon_i - \varepsilon_f)$ and $\int \mathrm{d}^3\mathbf{Q}\, \delta^{(3)}(\mathbf{Q} + \mathbf{p}'_\chi - \mathbf{p}_\chi)$ for the change of variables. In order to discuss the excitation process in the context of the response theory, we introduce the electron density operator $\hat{\rho}_e(\mathbf{x}) \equiv \hat{\psi}^\dagger_e(\mathbf{x})\hat{\psi}_e(\mathbf{x})$, where the nonrelativistic field operator $\hat{\psi}_e(\mathbf{x}) = \sum_j \hat{a}_j u_j(\mathbf{x})$ is expressed in terms of the eigen wavefunctions $\{u_j(\mathbf{x})\}$ and their corresponding creation (annihilation) operators $\left\{\hat{a}^\dagger_j\right\}$ ($\{\hat{a}_j\}$). In the momentum space, the density operator is rewritten as $\rho_{\mathbf{Q}} \equiv \int \mathrm{d}^3\mathbf{x} \hat{\rho}_e(\mathbf{x}) e^{-i\mathbf{Q}\cdot\hat{\mathbf{x}}}$, which describes the density fluctuation of the electron system [84]. The the dynamic structure factor is defined as

$$
\begin{aligned}
S_{\hat{\rho}\hat{\rho}}(\mathbf{Q},\omega) &= \frac{2\pi}{V_{\text{target}}}\sum_{i,f}\mathcal{P}_i\left|\langle f\,|\hat{\rho}_{-\mathbf{Q}}|\,i\rangle\right|^2\delta\left(\omega+\varepsilon_i-\varepsilon_f\right) \\
&= i\,\frac{\left[\chi_{\hat{\rho}\hat{\rho}}\left(\mathbf{Q},\omega+i0^+\right)-\chi_{\hat{\rho}\hat{\rho}}\left(\mathbf{Q},\omega-i0^+\right)\right]}{1-e^{-\beta\omega}} \\
&\simeq i\,\left[\chi_{\hat{\rho}\hat{\rho}}\left(\mathbf{Q},\,\omega+i0^+\right)-\chi_{\hat{\rho}\hat{\rho}}\left(\mathbf{Q},\,\omega-i0^+\right)\right]
\end{aligned}
$$

$$
= -2\,\mathrm{Im}\left[\chi^{\mathrm{r}}_{\hat{\rho}\hat{\rho}}\left(\mathbf{Q},\,\omega\right)\right] \tag{S.4}
$$

$$
= \frac{2}{V_{\text{Cou}}(\mathbf{Q})}\,\mathrm{Im}\left[\frac{-1}{\epsilon\left(\mathbf{Q},\omega\right)}\right], \tag{S.5}
$$

where $1-e^{-\beta\omega}$ depends on the inverse temperature $\beta = 1/k_B T$, which can be approximated as 1 for the semiconductor target. The master function $\chi_{\hat{\rho}\hat{\rho}}\left(\mathbf{Q},\,z\right)$, representing the correlation function of density operator $\hat{\rho}\hat{\rho}$, can be estimated by the Matsubara Green's function, and $\chi^{\mathrm{r}}_{\hat{\rho}\hat{\rho}}\left(\mathbf{Q},\,\omega\right) = \chi_{\hat{\rho}\hat{\rho}}\left(\mathbf{Q},\,\omega+i0^+\right)$ and $\chi_{\hat{\rho}\hat{\rho}}\left(\mathbf{Q},\,\omega-i0^+\right)$ are the corresponding retarded and advanced correlation function. For the last line, we use the relation between the dielectric function and retarded correlation function in the linear response theory, that is

$$
\frac{1}{\epsilon\left(\mathbf{Q},\omega\right)} = 1 + V_{\text{Cou}}\left(\mathbf{Q}\right)\chi^{\mathrm{r}}_{\hat{\rho}\hat{\rho}}\left(\mathbf{Q},\,\omega\right). \tag{S.6}
$$

In the nonrelativistic limit, the cross section in Eq. (S.1) reduces to the expression in Ref. [53], which describes the scattering between a halo DM particle and the electrons in solids.

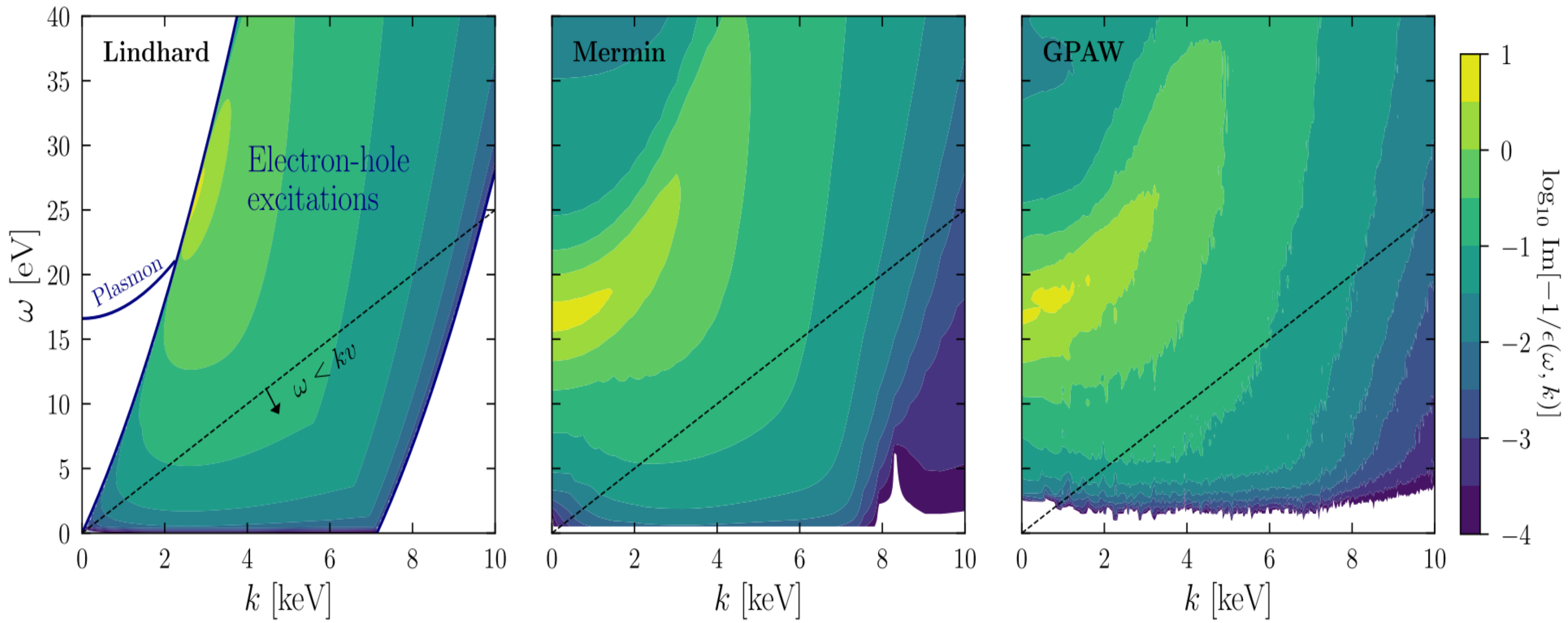

➢ The Lindhard method:

Assuming homogenous material and neglecting all dissipation effects.

➢ The Mermin method:

A generalization of the Lindhard which includes dissipation.

➢ The GPAW method:

It relies on a first principles calculation with package GPAW.

Simon Knapen, Jonathan Kozaczuk, and Tongyan Lin, Phys. Rev. D **105**, 015014(2021).

e.g. Cosmic Ray DM

$$\frac{\mathrm{d}\Phi_\chi}{\mathrm{d}T_\chi} \equiv D_{\mathrm{eff}} \frac{\rho_\chi^{\mathrm{local}}}{m_\chi} \int_{T_{\mathrm{CR}}^{\mathrm{min}}}^{\infty} \mathrm{d}T_{\mathrm{CR}} \frac{\mathrm{d}\sigma}{\mathrm{d}T_\chi} \frac{\mathrm{d}\Phi_{\mathrm{CR}}^{\mathrm{LIS}}}{\mathrm{d}T_{\mathrm{CR}}}$$

differential electronic excitation rate:

$$\begin{aligned}\frac{\mathrm{d}R}{\mathrm{d}\omega} &= \frac{1}{M_{\mathrm{target}}} \int \mathrm{d}E_\chi \int \frac{\mathrm{d}\Omega}{4\pi} \frac{\mathrm{d}\Phi_\chi}{\mathrm{d}E_\chi} \frac{\mathrm{d}\sigma}{\mathrm{d}\omega} \\ &= \frac{1}{\rho_T} \frac{\bar{\sigma}_{\chi e}}{4\alpha\mu_{\chi e}^2} \int \frac{\mathrm{d}^3\mathbf{Q}}{(2\pi)^3} \int \mathrm{d}E_\chi \frac{\mathrm{d}\Phi(E_\chi)}{\mathrm{d}E_\chi} \left(\frac{(2E_\chi - \omega)^2 - Q^2}{4E_\chi(E_\chi - \omega)}\right) \left(\frac{\alpha^2 m_e^2 + m_{A'}^2}{Q^2 - \omega^2 + m_{A'}^2}\right)^2 \left(\frac{E_\chi(E_\chi - \omega)}{p_\chi^2}\right) \\ &\times Q\, \mathrm{Im}\left[\frac{-1}{\epsilon(\mathbf{Q},\omega)}\right] \Theta\left[E_\chi - \sqrt{(p_\chi - Q)^2 + m_\chi^2} - \omega\right],\end{aligned}$$

DM-Electron scattering in semiconductor

- Comparison with EELS data:

The results an incident electron beam kinetic energy of $T = 100$ keV

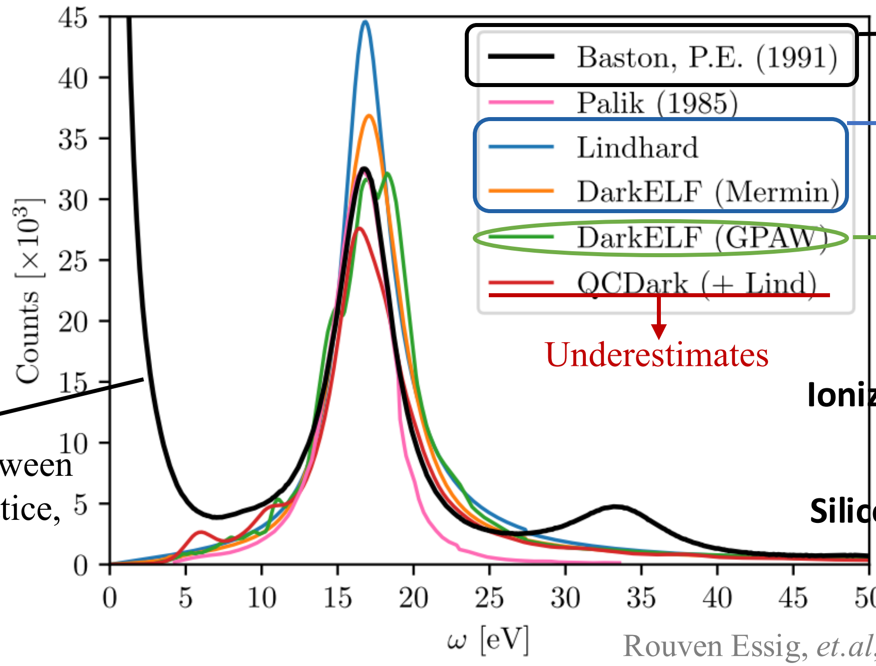

The data of EELS

Overestimating the response

The position and height of peak is consistent, but GPAW predicts a slightly broader peak.

Underestimates

The elastic scattering between incident electrons and lattice, not electron-hole pair excitations.

Rouven Essig, *et.al*, arxiv: 2403.00123

Ionization charge: $\mathcal{Q}(\omega) = 1 + \lfloor (\omega - E_{\rm gap})/\varepsilon \rfloor$

1509.01598

Silicon: E_{gap} = 1.2eV and ε = 3.8eV.

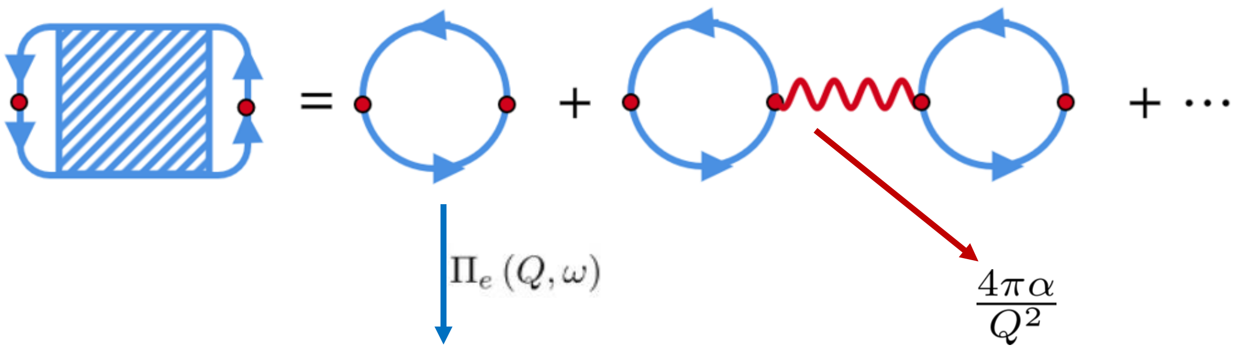

$$\frac{1}{V}\sum_{i,j}\frac{\left|\langle i|e^{i\mathbf{Q}\cdot\hat{\mathbf{x}}}|j\rangle\right|^2}{\varepsilon_i-\varepsilon_j-\omega-i0^+}\left(f_i-f_j\right)$$

Lindhard function

$$\Gamma\left(\mathbf{p}_\chi\right)=\int\frac{\mathrm{d}^3\mathbf{Q}}{(2\pi)^3}\left|V(\mathbf{Q},\omega)\right|^2\left[2\frac{Q^2}{e^2}\mathrm{Im}\left(-\frac{1}{\epsilon(\mathbf{Q},\omega)}\right)\right]$$

- Similar Fermi's Golden Rule, but different kinematics

$$Q=|\mathbf{Q}|=\left|\mathbf{p}_\chi-\mathbf{p}_\chi'\right|,\quad \omega=E_\chi-E_\chi'=\sqrt{p_\chi^2+m_\chi^2}-\sqrt{\left|\mathbf{p}_\chi-\mathbf{Q}\right|^2+m_\chi^2}$$

- Scattering potential

$$\left|V(\mathbf{Q},\omega)\right|^2=\frac{\pi\bar{\sigma}_{\chi e}\left[\left(2E_\chi-\omega\right)^2-Q^2\right]}{4\mu_{\chi e}^2E_\chi\left(E_\chi-\omega\right)}\left|F_{\mathrm{DM}}(q)\right|^2,$$

- Dielectric function remains the same
- Event rate

$$R=\frac{1}{\rho_T}\int\mathrm{d}T_\chi\int\frac{\mathrm{d}\Omega}{4\pi}\frac{\mathrm{d}\Phi_\chi}{\mathrm{d}T_\chi}\left(\frac{E_\chi}{p_\chi}\right)\Gamma\left(p_\chi\right)$$

Cosmological and Astrophysical Constraints

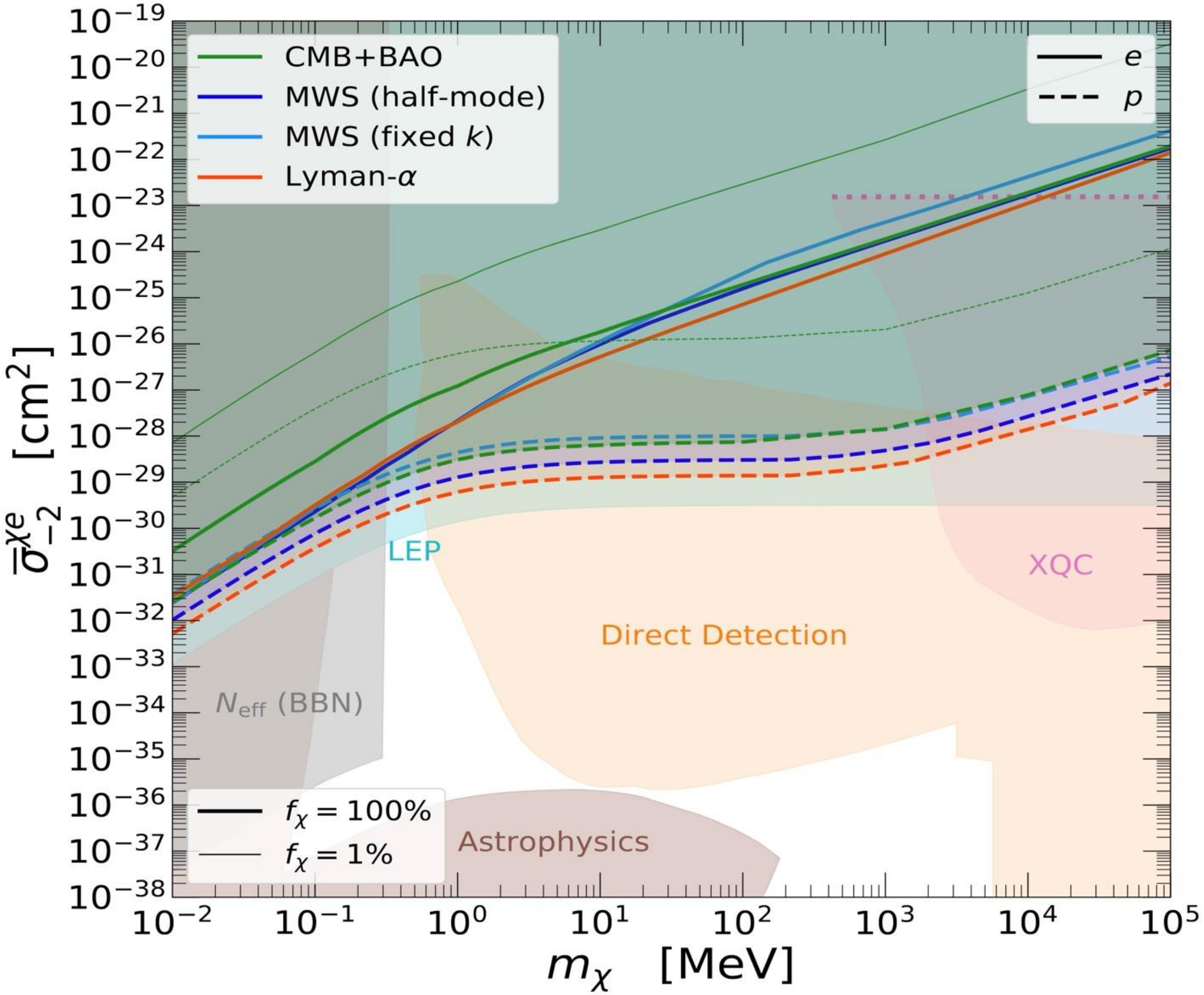

Neutrino Fog